

Boosting photocatalytic efficiency of iridium polypyridyl complex in coupling reaction through induction of ferrocene: New insights into bimetallic catalysis

Firdaus Rahaman Gayen,^{1,2} Sakshi Chawla,³ Debashree Bora,^{1,2} Lodsna Borkotoky,^{2,4} Sarifuddin Gazi,⁵ Dibyendu Mallick,⁶ Ram Awatar Maurya,^{2,4} Arijit Kumar De,^{*3} Biswajit Saha^{*1,2}

¹Advanced Materials Group, Materials Sciences and Technology Division, CSIR – North East Institute of Science and Technology, Jorhat, Assam – 785006, India

²Academy of Scientific and Innovative Research (AcSIR), Ghaziabad – 201002, India

³Department of Chemical Sciences, Indian Institute of Science Education and Research Mohali, Knowledge City, Sector 81, SAS Nagar, Punjab 140 306, India

⁴Applied Organic Chemistry Group, Chemical Sciences and Technology Division, CSIR – North East Institute of Science and Technology, Jorhat, Assam – 785006, India

⁵Department of Chemistry, University of Science & Technology Meghalaya (USTM), Meghalaya – 793101, India

⁶Department of Chemistry, Presidency University, Kolkata – 700073, India

**Email: bsaha@neist.res.in, bischem@gmail.com, akde@iisermohali.ac.in*

Table of Contents

1. General Experimental Section

2. Synthesis and characterization of cyclometalated iridium complex, $[\text{Ir}(\text{ppy})_2\text{Cl}]_2$ (1)

Figure S1. HRMS spectrum of 1

3. Synthesis and characterization of 4-ferrocenyl-2,2'-bipyridine ligand (fcbpy)

Scheme S1. Synthesis of fcbpy

Figure S2. ^1H NMR spectrum of fcbpy

Figure S3. ^{13}C NMR spectrum of fcbpy

Figure S4. HRMS spectrum of fcbpy

4. Synthesis and characterization of $[\text{Ir}(\text{ppy})_2(\text{fcbpy})]\text{PF}_6$ (2)

Figure S5. ^1H NMR spectrum of 2

Figure S6. ^{13}C NMR spectrum of 2

Figure S7. ^{19}F NMR spectrum of 2

Figure S8. ^{31}P NMR spectrum of 2

Figure S9. HRMS spectrum of 2

Figure S10. FT-IR spectrum of 2

Figure S11. CV of bipyridine (bpy)

Figure S12. CV of fcbpy

Figure S13. DPV of 2

5. X-ray data collection and refinement

Table S1. Crystallographic data and pertinent refinement parameters 2

Table S2. Bond distance and angle of 2

6. Calculation of excited state redoxpotentials of 2

Figure S14. Normalized UV-Visible and photoluminescence spectra of 2

Figure S15. Frontier Orbitals of Complex 2

Table S3. TDDFT data of complex 2

7. Details of the light source used in the photocatalysis

Figure S16. Photograph of the micro flowreactor setup

Figure S16A. Photocatalysis by 2 at continuous flow microreactor

8. General procedure for the synthesis of phenacylazides (3.7)

Scheme S1 Synthesis of phenacylazides 3.7

9. Handling of azides

10. General procedure for the synthesis of α -ketovinylazides (3.4)

Scheme S2 Synthesis of α -ketovinylazides 3.4

11. General procedure for the synthesis of (3,6-diphenyl-1,3-diazabicyclo[3.1.0]hexan-5-yl)(phenyl)methanones (3.6a-l)

Scheme S3 Photochemical coupling of 3.4 and 3.5 to yield 3.6 in presence of ferrocenyl iridium(III) complex as catalyst

12A. Characterization of (2-(4-chlorophenyl)-2H-azirin-3-yl)(4-methoxyphenyl)methanone

12B. Characterization of (3,6-diphenyl-1,3-diazabicyclo[3.1.0]hexan-5-yl)(phenyl)methanones

13. ^1H NMR and ^{13}C NMR Spectra of (3,6-diphenyl-1,3-diazabicyclo[3.1.0]hexan-5-yl)(phenyl)methanones

14. Details for spectroscopic measurements and transient absorption studies

- (a) Sample preparation for spectroscopic measurements
- (b) Steady-state and time-resolved emission measurements
- (c) Quantum yield measurements
- (d) Stern-Volmer measurements

Figure S19. Steady state excitation spectrum of complex **2** in deaerated ACN at two different emission bands (a) $\lambda_{\text{ex}} = 380$ nm and (b) $\lambda_{\text{ex}} = 600$ nm.

Figure S20. Steady state emission spectrum of (a) $[\text{Ir}(\text{ppy})_2(\text{bpy})]\text{PF}_6$ ($\lambda_{\text{ex}} = 355$ nm) and (b) $[\text{Ir}(\text{ppy})_2(\text{fcbpy})]\text{PF}_6$ ($\lambda_{\text{ex}} = 400$ nm) in deaerated ACN with increasing concentrations of N,N-dimethylaniline and (c) Comparison plot for Stern-Volmer quenching as a function of concentration of N,N-dimethylaniline, along with the experimental fit.

Figure S21. Steady state emission spectrum of (a) $[\text{Ir}(\text{ppy})_2(\text{bpy})]\text{PF}_6$ ($\lambda_{\text{ex}} = 355$ nm) and (b) $[\text{Ir}(\text{ppy})_2(\text{fcbpy})]\text{PF}_6$ ($\lambda_{\text{ex}} = 400$ nm) in deaerated ACN with increasing concentrations of N,N-dimethylaniline and (c) Comparison plot for Stern-Volmer quenching as a function of concentration of α -ketovinylazide along with the experimental fit.

Table S4. Time constant for Stern-Volmer and bimolecular fluorescence quenching.

- (e) Transient absorption measurements
- (f) TA data analysis

Figure S22. (a) TA spectral traces at early probe delays, (b) Spectral traces at later time delays, (c) EADS and (d) Population dynamics for complex **[Ir(ppy)₂(bpy)](PF₆)** in ACN following 400 nm excitation.

Figure S23. Kinetic traces at selected wavelengths showing the best fits for complex **[Ir(ppy)₂(bpy)](PF₆)** in ACN.

Figure S24. (a) Kinetic traces at selected wavelengths showing the best fits for complex **[Ir(ppy)₂(fcbpy)](PF₆)** in ACN and (b) Zoomed kinetic traces at longer time delay.

Figure S24. The comparison of $E_{1/2}$, $E_{1/2}^*$ and lifetime of the catalysts (Ir-complexes)

Table S5. Time constants obtained from the global analysis of the TA data.

15. Computational Details

16. References

1. General Experimental Section

All reactions were carried out oven dried glassware and in open air except fcbpy synthesis. The 36 W white light CFL and 15 W LED bulbs commonly used for domestic lighting were used for this research. Isolation and purification of crude products were done by column chromatography in air using silica gel (200-300 mesh). All the chemicals were purchased from commercial suppliers (TCI, Sigma-Aldrich and Avra Chemicals) and used without further purification. Analytical thin-layer chromatography (TLC) was performed using silica gel 60F254 plates and visualization was carried out with UV light. ^1H NMR (500 MHz), ^{13}C NMR (125 MHz), ^{31}P NMR (202 MHz) and ^{19}F NMR (471 MHz) were recorded at room temperature on a Bruker Advance 500 MHz spectrometer using TMS as an internal standard. Chemical shifts are reported in parts-per-million (ppm, δ) downfield from residual solvents peaks and coupling constants are reported as Hertz (Hz). Splitting patterns are designated as: s = singlet, d = doublet, t = triplet, q = quartet, m = multiplet etc. HRMS were recorded on a Q-TOF spectrometer (Xevo XS QToF mass spectrometer) in electrospray ionization mode. Absorption spectra were recorded on a UV-Vis spectrophotometer (Cary 5000 UV-Vis NIR, Agilent Technologies). Steady state emission spectra were recorded on a steady state fluorimeter (Cary Eclipse fluorescence spectrophotometer, Agilent Technologies). Time-resolved fluorescence lifetime was obtained using the time-correlated single photon counting (TCSPC) fluorimeter (Deltaflex, Horiba Scientific). Ultrafast TA studies were performed using a customized setup discussed in detail in ESI† (section 12). The voltametric analysis was carried out using conventional three electrode system (Working electrode: Platinum disk; Counter electrode: Platinum wire; Reference electrode: Ag/AgCl) by using BASI electrochemical analyzer (Epsilon Eclipse™, USA). Melting points were recorded using a melting point equipment M-500, BUCHI Labortechnik

AGCH-9230 Flawil 1, Switzerland. FT-IR spectra were recorded on a Perkin Elmer Spectrum 100 spectrometer with KBr pellet in the frequency range of 4000-400 cm^{-1} . Elemental analyses were conducted on a CHN analyzer PE-2400 (Perkin Elmer, USA).

2. Synthesis and characterization of cyclometalated iridium complex, [Ir(ppy)₂Cl]₂(1)

In a 25 mL round bottomed (RB) flask, 2-phenylpyridine (0.169 mL, 1.18 mmol, 2.2 equiv.) was dissolved in 2-methoxyethanol (0.74 mL) before addition of IrCl₃.nH₂O (n = 4, 0.200 g, 0.53 mmol, 1.0 equiv.) and distilled water (2.5 mL). The reaction mixture was allowed to reflux at 120 °C for 16 h. A bright yellow color product was formed during the reaction. The reaction mixture was cooled to room temperature after completing the reflux and mixed with distilled water (20 mL). Vacuum filtration was used to isolate the product and washed with water (3 x 10 mL) followed by drying in high vacuum. A yellow color solid product was obtained which was further triturated by hexane and dried well in high vacuum to get the pure product [Ir(ppy)₂Cl]₂ (1.08 g, 85% yield) which can be used without further purification. HRMS (ESI-TOF-Q) calculated for C₂₂H₁₆IrN₂: 501.0942, found: 501.1689 [M/2]⁺.¹

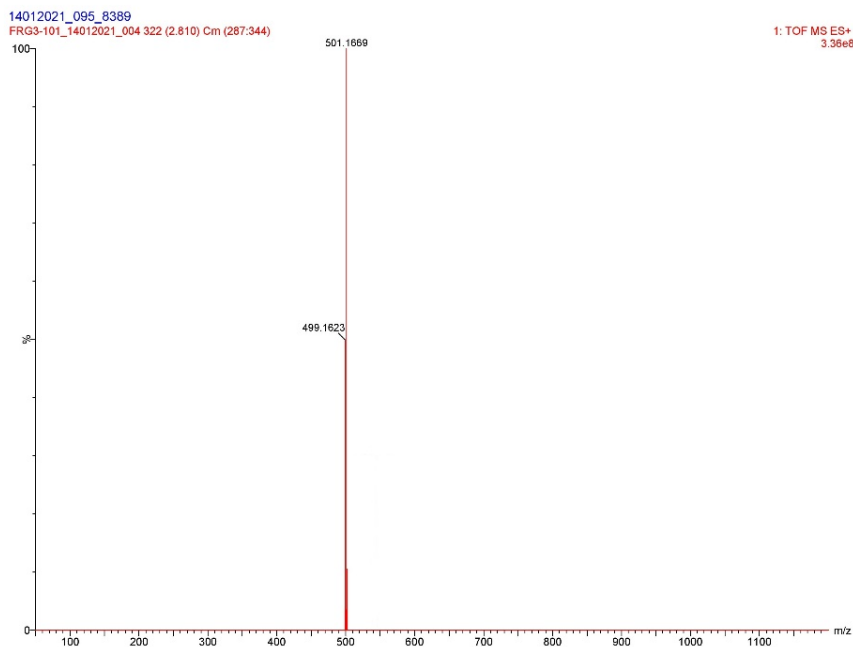
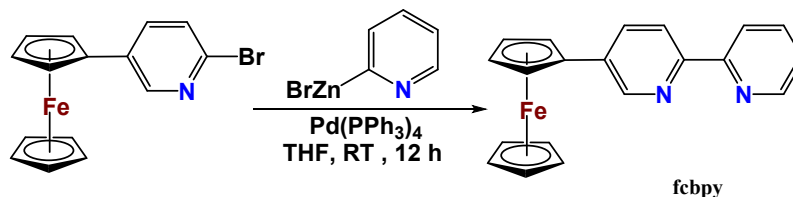


Figure S1.HRMS spectrum of 1

3. Synthesis and characterization of 4-ferrocenyl-2,2'-bipyridine ligand (fcbpy)



Scheme S1. Synthesis of **fcbpy**

5-ferrocenyl-2-bromo-pyridine (0.500 g, 1.4 mmol, 1.0 equiv.), Pd(PPh₃)₄ (0.050 g, 0.04 mmol, 0.03 equiv.) and dry THF (5 mL) were filled into a 100 mL flame dried Schlenk flask with magnetic stir bar and purged with argon gas. Then the mixture was stirred for 30 min at room temperature resulting in yellow-orange slurry. Later 2-pyridylzinc bromide (7.3 mL, 3.6 mmol 0.5 M solution in THF) was added by syringe and the flask was sealed with rubber septa. The reaction mixture was stirred at room temperature for 12 h. Then aqueous HCl was added (3.0 M; 2.5 mL) to blood red color reaction mixture. Later aqueous NaOH (25 wt.%, 2.5 mL) was added followed by an extraction of the product with Et₂O (100 mL), washed with 10 mL of saturated aqueous NaCl. Then the combined organic extract was dried over Na₂SO₄ and filtered. Later the solvent was removed in vacuo and the crude product was purified by flash column chromatography on silica gel using Hexane/EtOAc, starting with 9:1 v/v and increasing the gradient to 8:2 v/v. Finally, removal of the solvent in vacuo gave the compound as a bright orange-red powder (0.355 g, 71% yield). ¹H NMR (500 MHz, CDCl₃): δ (ppm) = 8.75 (dd, *J* = 2.3, 0.9 Hz, 1H, Ar-H), 8.62 (ddd, *J* = 4.8, 1.8, 1.0 Hz, 1H, Ar-H), 8.33 (dt, *J* = 8.0, 1.1 Hz, 1H, Ar-H), 8.26 (dd, *J* = 8.2, 0.8 Hz, 1H, Ar-H), 7.83 – 7.72 (m, 2H, Ar-H), 7.24 (ddd, *J* = 7.5, 4.8, 1.2 Hz, 1H, Ar-H), 4.68 (t, *J* = 1.9 Hz, 2H, Cp-H), 4.38 – 4.33 (m, 2H, Cp-H), 4.01 (s, 5H, Cp-H). ¹³C NMR (125 MHz, CDCl₃) δ (ppm) = 156.1, 153.4, 149.2, 146.6, 136.9, 135.8, 133.8, 123.4, 120.7, 120.6 (Ar-C); 81.2, 69.8, 69.7, 66.5 (Cp-C). FT-IR (KBr pellet, cm⁻¹): 3043, 1574,

1434, 1098, 804, 504. UV-Visible [λ_{max} , (CH₃CN), nm]: 254, 307, 372, 456. HRMS (ESI-TOF-Q) calculated for C₂₀H₁₆FeN₂ [fcbpy+H]⁺: 341.0741, found: 341.2104 [fcbpy+H]⁺. M.p. 185-188 °C; Anal. Calcd for C₂₀H₁₆FeN₂: C, 70.61; H, 4.74; N, 8.23. Found: C, 70.58; H, 4.72; N, 8.20.

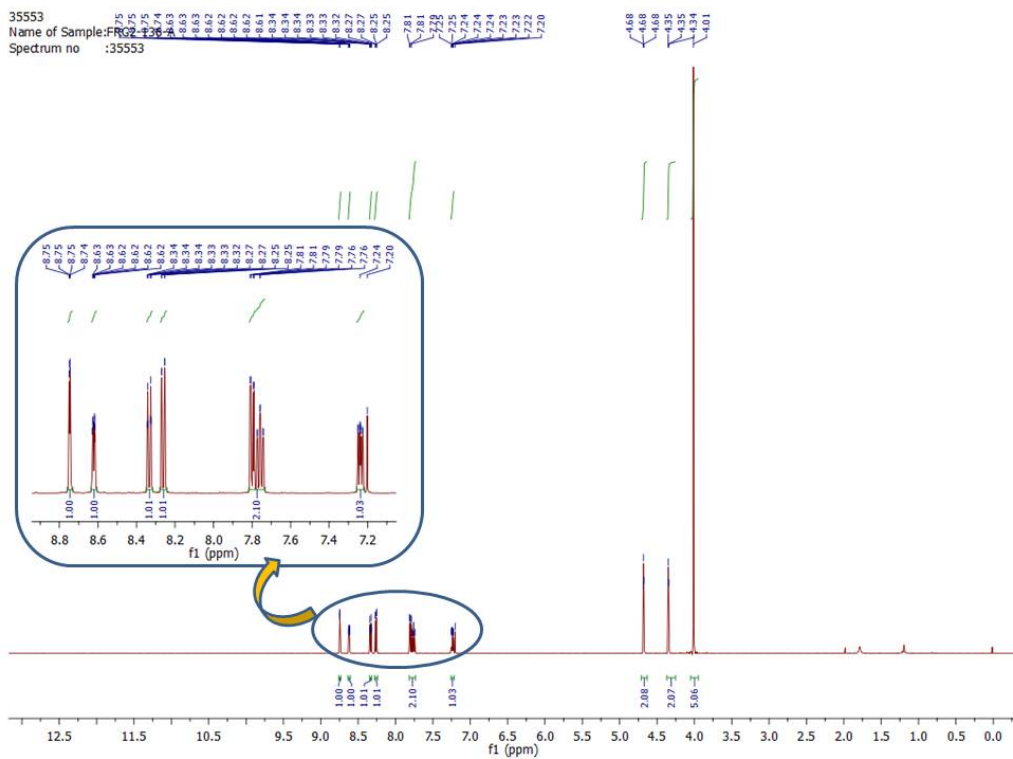


Figure S2. ¹H NMR spectrum of fcbpy

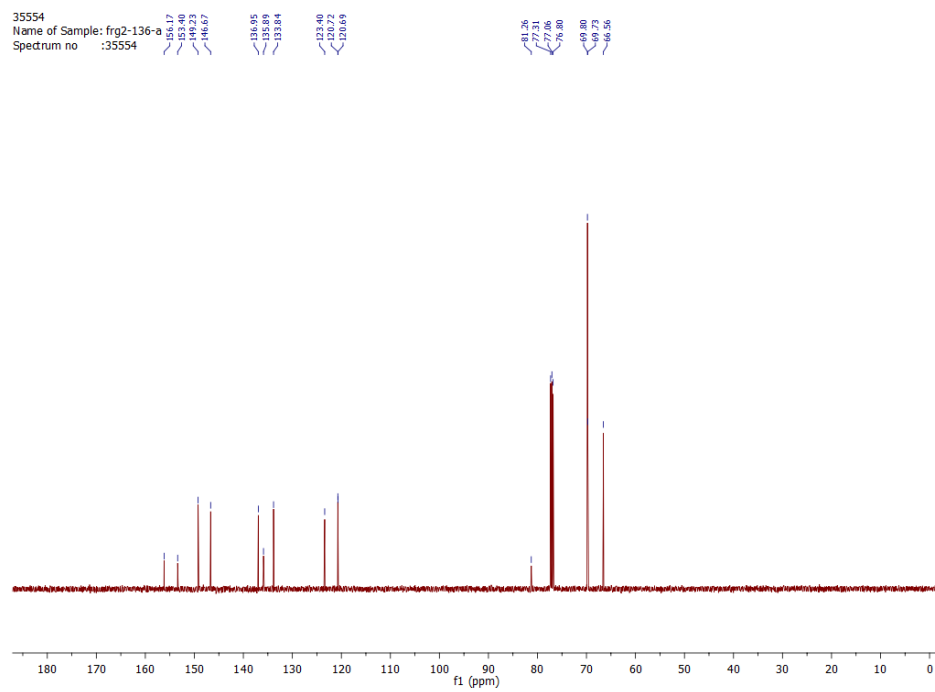


Figure S3. ¹³C NMR spectrum of fcbpy

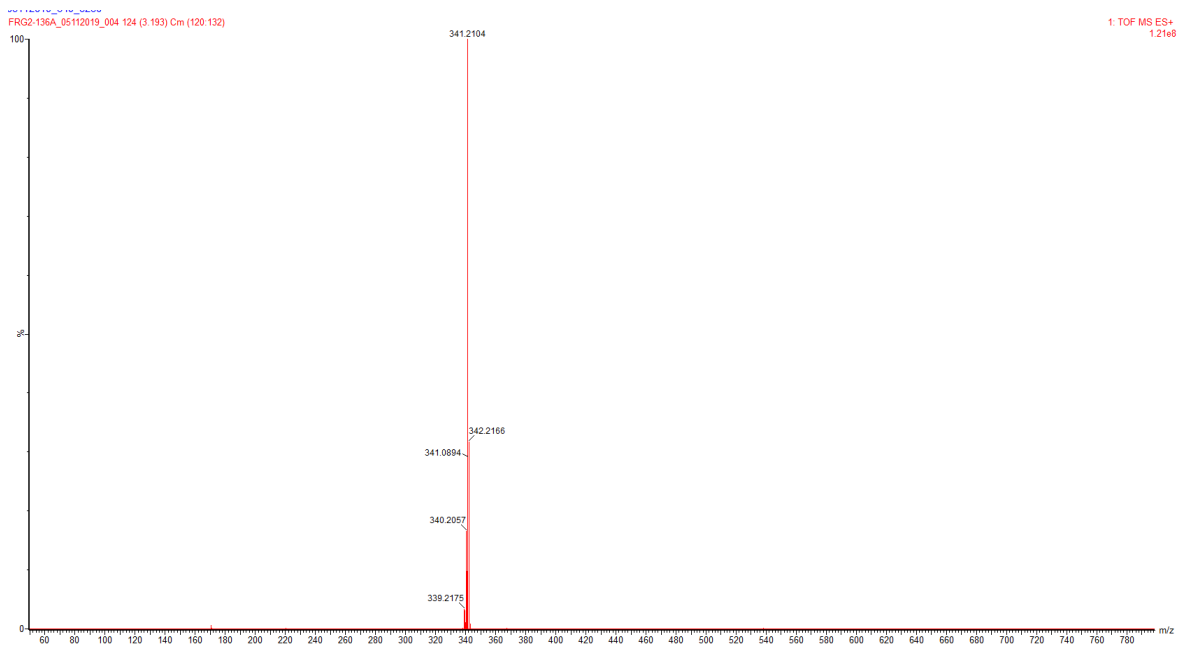


Figure S4. HRMS spectrum of fcbpy

4. Synthesis and characterization of [Ir(ppy)₂(fcbpy)]PF₆ (2)

A mixture of [Ir(ppy)₂Cl]₂ (0.100 g, 0.09 mmol, 1.0 equiv.), fcbpy (0.072 g, 0.2 mmol, 2.3 equiv.) were taken in a 25 mL RB flask and dissolved in 3 mL ethylene glycol. The reaction mixture was allowed to reflux at 150 °C for 12 h. The reaction mixture was cooled to room temperature and poured into distilled water (75 mL). The aqueous solution of reaction was extracted by diethyl ether (3 x 20 mL) and the aqueous part was collected followed by heated at 70 °C. A solution of NH₄PF₆ (0.304g, 1.86 mmol, 20.0 equiv.) in water (5 mL) was added into the heated aqueous solution carefully. The reaction mixture was allowed to cool at ~5 °C for 1 h. A deep red color precipitate was observed during the step which was isolated by vacuum filtration followed by washed with water (2 x 20 mL) and dried under high vacuum. The product was isolated via recrystallization by dissolving into acetonitrile (1.0 mL) in a 30 mL vial, which is placed in a secondary container of diethyl ether (30 mL) for 12 h. The pure product was obtained by decanting the supernatant followed by washing with diethyl ether (2 x 10 mL) and dried under high vacuum. Yield: 0.080 g, 88% yield. ¹H NMR (500 MHz, CDCl₃) δ (ppm) = 8.53 (d, *J* = 8.2 Hz, 1H, Ar-H), 8.42 (d, *J* = 8.6 Hz, 1H, Ar-H), 8.07 – 8.01 (m, 1H, Ar-H), 7.93 (d, *J* = 8.5 Hz, 1H, Ar-H), 7.91 (s, 1H, Ar-H), 7.89 – 7.83 (m, 3H, Ar-H), 7.73 – 7.67 (m, 3H, Ar-H), 7.65 (d, *J* = 6.3 Hz, 1H, Ar-H), 7.54 (dd, *J* = 14.2, 5.1 Hz, 2H, Ar-H), 7.31 (dd, *J* = 8.2, 6.1 Hz, 1H, Ar-H), 7.13 – 7.07 (m, 1H, Ar-H), 7.04 – 6.94 (m, 4H, Ar-H), 6.87 (d, *J* = 6.1 Hz, 1H, Ar-H), 6.35 – 6.30 (m, 2H, Ar-H), 4.38 – 4.31 (m, 3H, Cp-H), 4.26 (d, *J* = 1.8 Hz, 1H, Cp-H), 3.73 (s, 5H, Cp-H). ¹³C NMR (126 MHz, CDCl₃) δ (ppm) = 167.7, 155.9, 151.5, 151.0, 150.4, 149.9, 148.6, 148.3, 147.4, 143.4, 143.3, 142.2, 139.6, 138.0, 134.9, 131.8, 131.7, 130.8, 130.7, 127.1, 124.9, 124.7, 123.4, 123.2, 122.7, 122.5, 119.5, 119.4 (Ar-C); 71.0, 70.0, 66.9, 66.6 (Cp-C). FT-IR (KBr pellet, cm⁻¹): 3437, 1609, 1479, 842, 557. UV-Visible [λ_{max} , (CH₃CN), nm]: 256, 324,

524.HRMS (ESI-TOF-Q) calculated for $C_{42}H_{32}FeIrN_4$: 841.1605, found: 841.1704 [**2**-PF₆]⁺.

M.p. 280 – 282 °C; Anal. Calcd for $C_{42}H_{32}F_6FeIrN_4PC$, 51.17; H, 3.27; N, 5.68; Found: C, 51.15;

H, 3.24; N, 5.65.

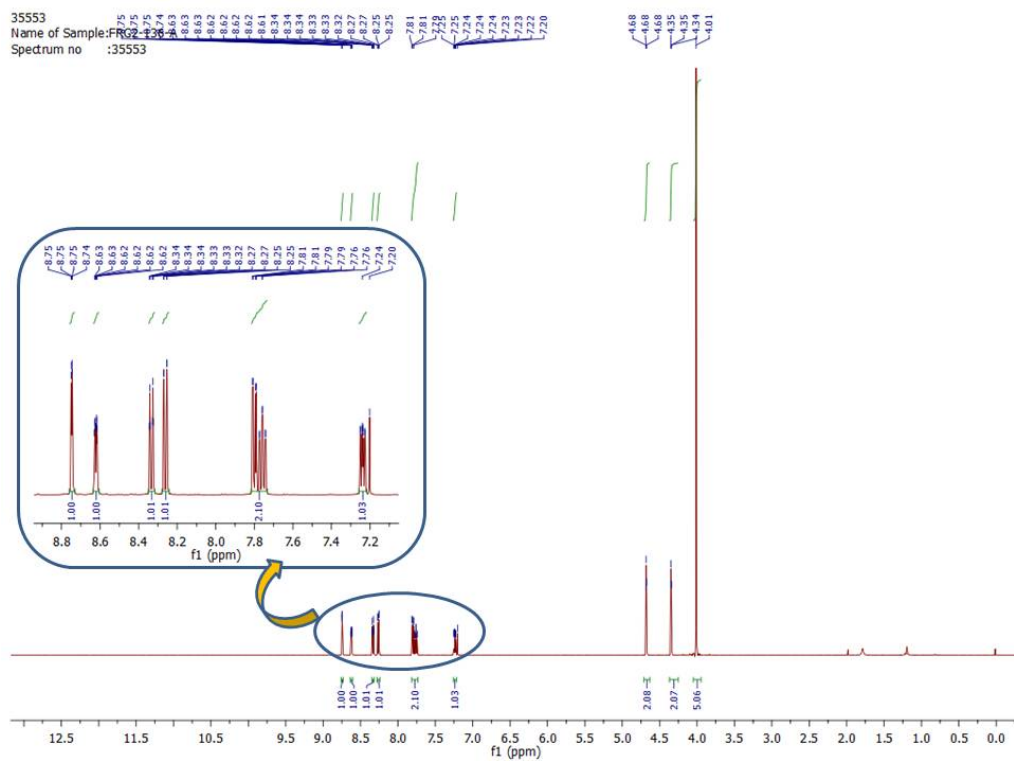


Figure S5. ^1H NMR spectrum of **2**

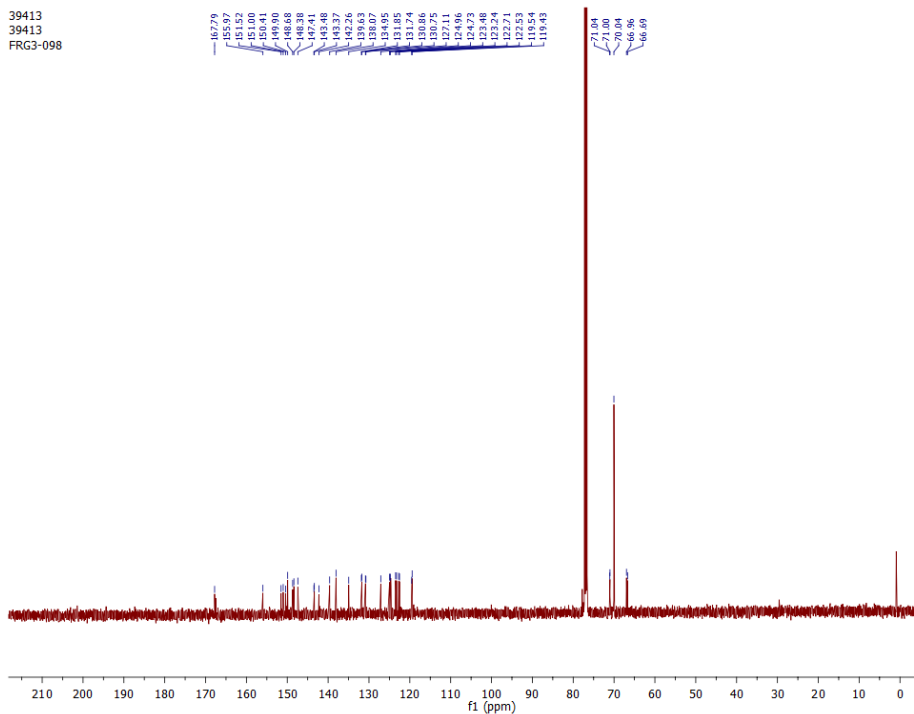


Figure S6. ^{13}C NMR spectrum of **2**

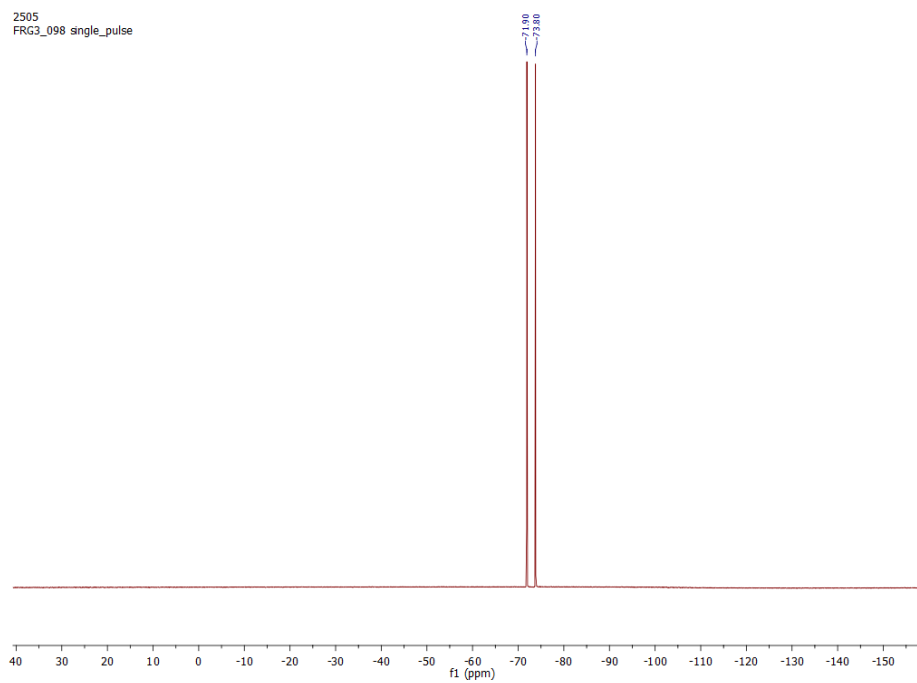


Figure S7. ^{19}F NMR spectrum of **2**

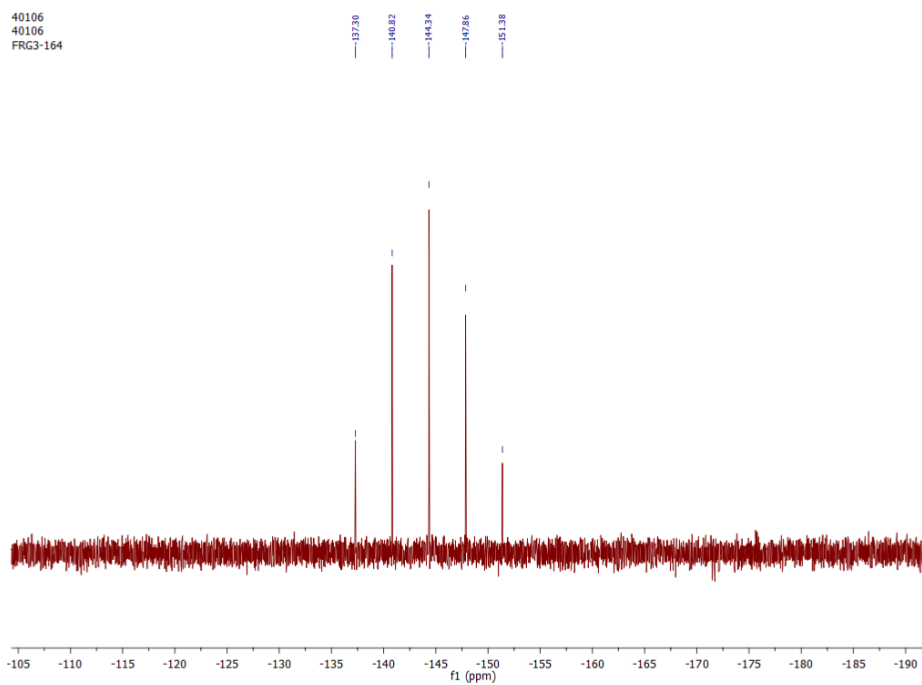


Figure S8. ^{31}P NMR spectrum of **2**

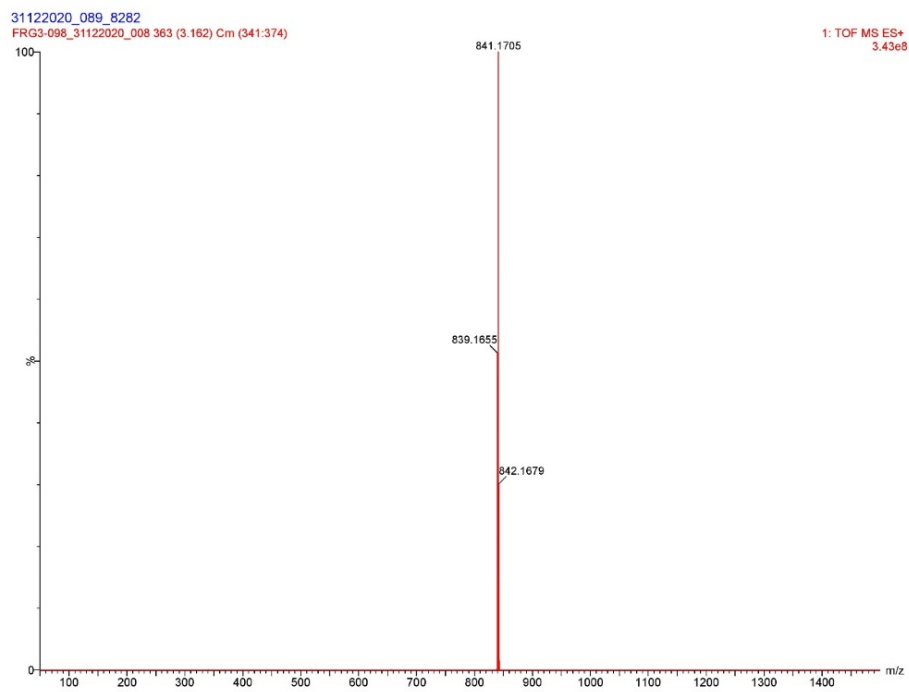


Figure S9. HRMS spectrum of 2

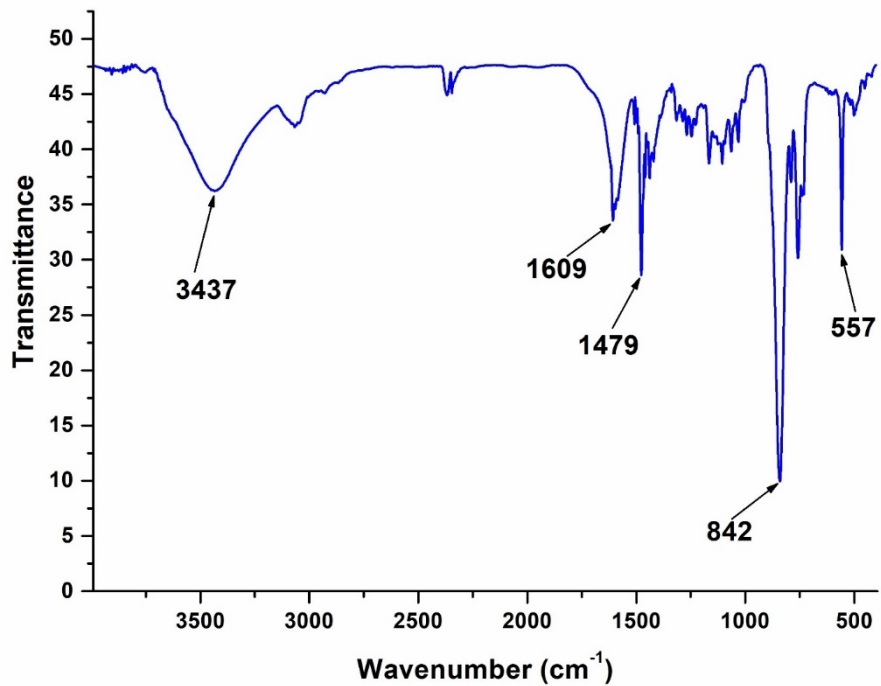


Figure S10. FT-IR spectrum of 2

5. X-ray data collection and refinement

Single-crystal X-ray studies were performed on a CCD Bruker SMART APEX diffractometer equipped with an Oxford Instruments low-temperature attachment. All the data were collected at 100(2) K using graphite-monochromated MoK $_{\alpha}$ radiation ($\lambda_{\alpha} = 0.71073 \text{ \AA}$). The frames were indexed, integrated, and scaled by using the SMART and SAINT software packages² and the data were corrected for absorption by using the SADABS program.³ The structures were solved and refined with the SHELX suite of programs.⁴ All the hydrogen atoms were included in the final stages of the refinement and were refined with a typical riding model. Structure solution and refinement details for compound **2** are provided in Table S1. Pertinent crystallographic data for compound **2** is summarized in Table S2. The crystallographic figures used in this manuscript were generated using Diamond 3.1e software.⁵ CCDC –2213653 <http://www.ccdc.cam.ac.uk/cgi-bin/catreq.cgi> ‡ contain the supplementary crystallographic data for this paper.

Table S1. Crystallographic data and pertinent refinement parameters **2**

Empirical formula	C ₄₄ H ₃₂ F ₆ FeIrN ₄ P
Formula Weight	985.73
Crystal System	Monoclinic
Space Group	<i>P</i> 2 ₁ / <i>c</i>
<i>a</i> (Å)	16.71160(1)
<i>b</i> (Å)	14.07180(1)
<i>c</i> (Å)	15.44540(1)
α (deg)	90
β (deg)	96.0980(1)
γ (deg)	90
<i>V</i> (Å ³)	3611.62(4)
<i>Z</i>	4
ρ_{calcd} (g cm ⁻³)	1.813
μ (mm ⁻¹)	11.270
<i>F</i> (000)	1936
Reflections	
Collected	42163
Independent	6569
Observed [<i>I</i> >2 σ (<i>I</i>)]	6003
No. of variables	496
GooF	1.049
R _{int}	0.0947
Final R indices	R1 = 0.0338
[<i>I</i> > 2 σ (<i>I</i>)] ^a	wR2 = 0.0906
R indices (all data) ^a	R1 = 0.0364
	wR2 = 0.0925

^aR₁ = $\Sigma||F_o| - |F_c||/\Sigma|F_o|$ with $F_o^2 > 2\sigma(F_o^2)$. wR₂ = $[\Sigma w(|F_o^2| - |F_c^2|)^2/\Sigma|F_o^2|^{1/2}]^{1/2}$

Table S2.Bond distance and angle of**2**

Bond Distance (Å)	
Ir1-N1	2.042(3)
Ir1-N2	2.050(3)
Ir1-N3	2.143(3)
Ir1-N4	2.127(3)
Ir1-C11	2.008(4)
Ir1-C22	2.009(4)
Fe1-C36	2.051(4)
Fe1-C33	2.035(4)
Fe1-C41	2.046(4)
Fe1-C39	2.036(4)
P1-F1	1.598(3)
N2-C12	1.343(5)
N1-C1	1.350(5)
N3-C23	1.334(5)
N4-C28	1.361(5)
Bond Angle (°)	
N1-Ir1-N3	90.53(12)
N1-Ir1-N4	96.03(12)
N2-Ir1-N3	95.50(12)
N2-Ir1-N4	87.27(12)
N4-Ir1-N3	76.66(12)
C11-Ir1-N3	97.96(14)
C11-Ir1-N1	80.42(14)
C22-Ir1-N2	80.59(14)
C22-Ir1-N4	95.50(13)
C33-Fe1-C36	68.86(16)
C33-Fe1-C41	129.34(18)
C39-Fe1-C41	68.36(19)
C39-Fe1-C36	106.82(19)

Cyclic voltammetry Study

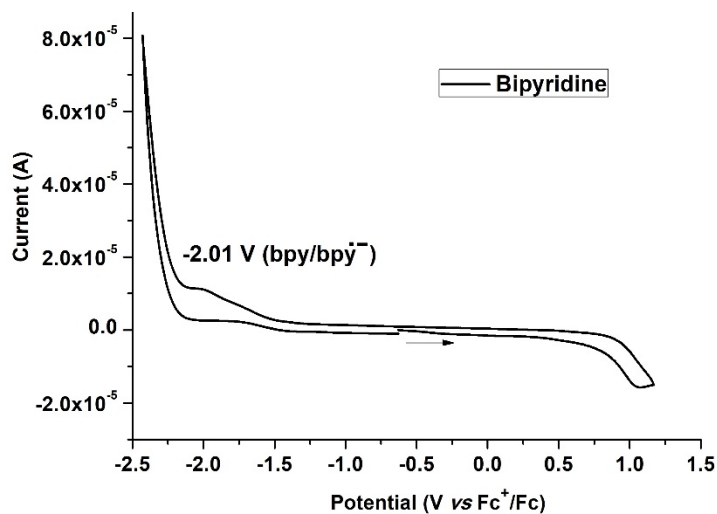


Figure S11. Cyclic voltammogram of bipyridine (bpy). $E_{1/2}$ (V); Reference electrode: ferrocene/ferrocenium (Fc/Fc^+); Solvent: acetonitrile; electrolyte 0.1 M TBAPF_6 ; $[\text{bpy}] = 0.001$ M; scan rate 100 mVs^{-1} ; RT.

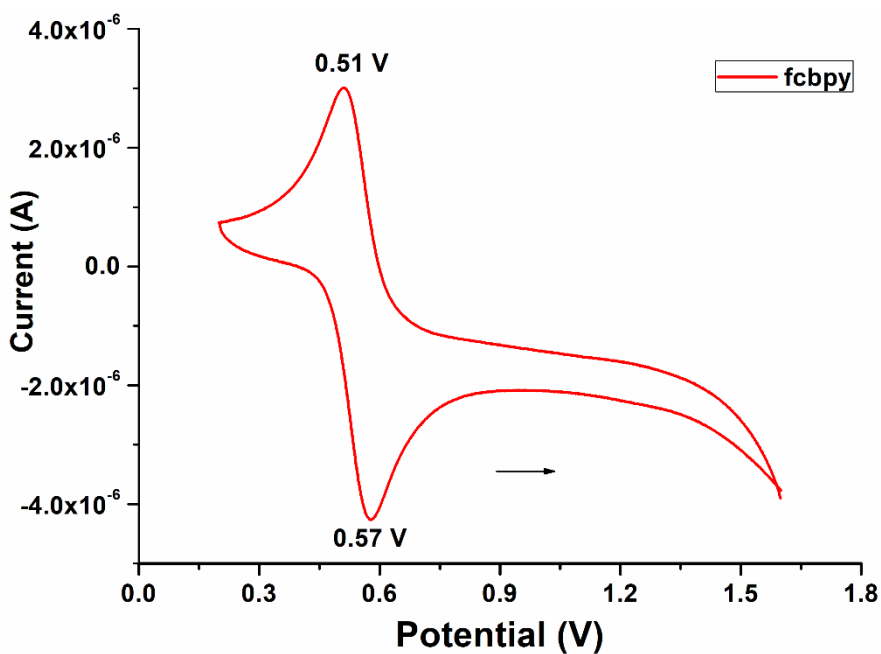


Figure S12. Cyclic voltammogram of fcbpy. Solvent: acetonitrile; electrolyte 0.1 M TBAPF_6 ; $[\text{fcbpy}] = 0.001$ M; scan rate 100 mVs^{-1} ; RT.

Differential pulse voltammogram of **2**.

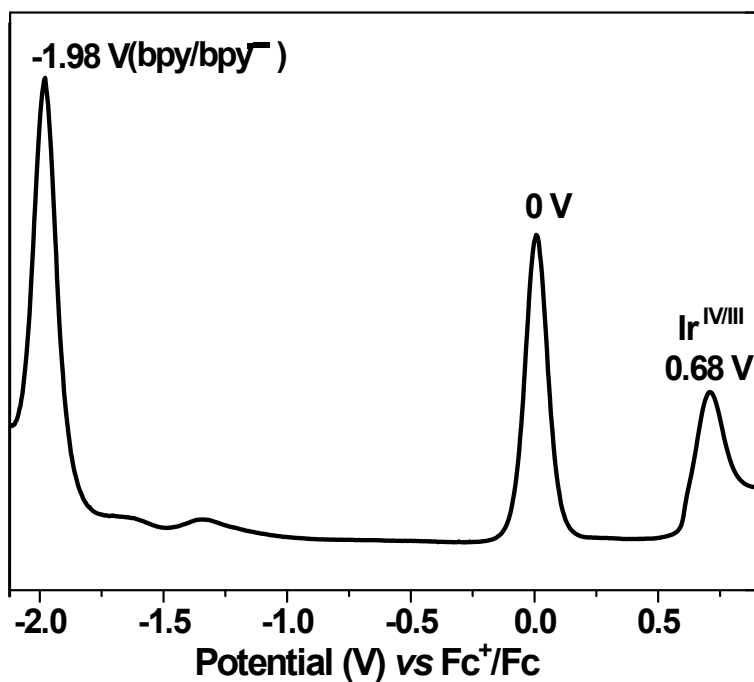


Figure S13. Differential pulse voltammogram of **2**. $E_{1/2}$ (V); Reference electrode: ferrocene/ferrocenium (Fc/Fc⁺); counter electrode: Platinum wire; working electrode: Platinum disc. Solvent: acetonitrile; electrolyte 0.1 M TBAPF₆; [**2**] = 0.001 M; scan rate 100 mVs⁻¹; RT.

6. Calculation of excited state redox potential of **2**

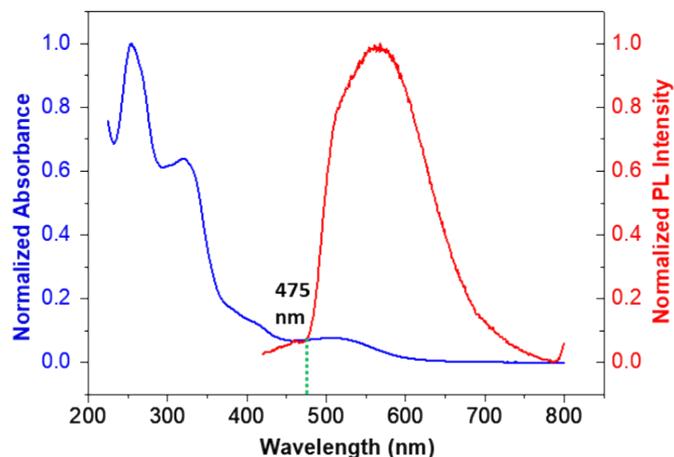


Figure S14. Normalized UV-Visible and photoluminescence spectra of **2** after excitation at 400 nm.

Calculation of Excited State Reduction Potential of **2**

The redox potentials at the excited state of a photocatalyst is calculated by Rehm and Weller equation involving its reduction and oxidation ground state potentials and the average energy of the zero-zero transitions that is calculated using wavelength at the crossing point of the normalized UV-Vis absorption and emission spectra.

It is found from the cyclic voltammogram of **2** (**Figure 3**) as well as from the differential pulse voltammogram (**Figure S13**) that the reversible reductive redox conversion of $[\text{Ir}(\text{ppy})_2(\text{fcbpy})]^+$ to $[\text{Ir}(\text{ppy})_2(\text{fcbpy})]^{+\cdot}$ i.e. (PC/PC $^{\cdot-}$) has started at -1.83 V and ended at -2.06 V vs Fc^+/Fc . Here, the redox potential of this reductive redox conversion has been considered as

$$\begin{aligned} E_{1/2}(\text{PC}/\text{PC}^{\cdot-}) &= -1.93 \text{ V vs } \text{Fc}^+/\text{Fc} \\ &= -1.55 \text{ V vs SCE} \end{aligned}$$

Again, from the Figure S14 it is clear that the normalized absorption and emission spectra of **2** are crossing at 475 nm.

The Gibbs Energy change associated with relaxation of the $^3\text{MLCT}$ excited state can be estimated from the PL spectrum of **2** ($\Delta G_0 \approx E = hc/\lambda$). Using the 475 nm the excited-state

energy can be estimated to be $\Delta G_0 \approx -251.85$ kJ/mole. Just as excitation can be thought of as a one-electron intermolecular redox reaction, so can luminescence.

Therefore, we can calculate a voltage associated with relaxation of the $^3\text{MLCT}$ excited state:

$$E_0 = -\Delta G_0 / nF = - (-251.85 \text{ kJ/mole}) / (1) (96.50) = +2.61 \text{ V vs NHE} = 2.366 \text{ V vs SCE}$$

Now,

We need to calculate excited state reduction potential $^*E^{\text{red}}$ (V vs SCE) of $^*2([\text{Ir}(\text{ppy})_2(\text{fcbpy})]^+)$ to $2([\text{Ir}(\text{ppy})_2(\text{fcbpy})]^{\cdot -})$ process.

For $^*[\text{Ir}(\text{ppy})_2(\text{fcbpy})]^+ \rightarrow [\text{Ir}(\text{ppy})_2(\text{fcbpy})]^+$, $E_0 = +2.366 \text{ V} \dots$ (Potential of relaxation from the $^3\text{MLCT}$ excited state).....eqn. 1

For, $[\text{Ir}(\text{ppy})_2(\text{fcbpy})]^+ + e \rightarrow [\text{Ir}(\text{ppy})_2(\text{fcbpy})]^{\cdot -}$ $E_0 = -1.55 \text{ V} \dots$ (Ground state reduction potential).....eqn. 2

By adding, eqn. 1 & 2 we get,

$$\begin{aligned} &^*[\text{Ir}(\text{ppy})_2(\text{fcbpy})]^+ + e \rightarrow [\text{Ir}(\text{ppy})_2(\text{fcbpy})]^{\cdot -} + ^*E^{\text{red}} \text{ (V vs SCE)} \\ &= (2.366 - 1.55) \text{ V vs SCE} = 0.815 \text{ V vs SCE} \end{aligned}$$

Hence, the complex **2** has excited state reduction potential, $^*E_{1/2}^{\text{red}}$ of 0.815 V vs SCE for $^*[\text{Ir}(\text{ppy})_2(\text{fcbpy})]^+$ to $[\text{Ir}(\text{ppy})_2(\text{fcbpy})]^{\cdot -}$ process.

Calculation of Excited State Oxidation Potential of 2

It is found from the cyclic voltammogram of **2** (**Figure 2**) that the ground state redox potential of the Ir(IV)/ Ir(III) redox couple

$$\begin{aligned} E_{1/2}(\text{Ir}^{\text{IV}}/\text{Ir}^{\text{III}}) &= \mathbf{0.68 \text{ V vs Fc}^+/\text{Fc}} \\ &= \mathbf{1.06 \text{ V vs SCE}} \end{aligned}$$

We need to calculate excited state oxidation potential $^*E^{\text{ox}}$ (V vs SCE) of $^*2(\text{Ir}^{\text{III}})$ to $2(\text{Ir}^{\text{IV}})$ process.

For $^*2(\text{Ir}^{\text{III}}) \rightarrow 2(\text{Ir}^{\text{IV}})$, $E_0 = +2.366 \text{ V} \dots$ (Potential of relaxation from the $^3\text{MLCT}$ excited state).....eqn. 1

For, $2(\text{Ir}^{\text{IV}}) + e \rightarrow 2(\text{Ir}^{\text{III}})$, $E_0 = 1.06 \text{ V} \dots$ (Ground state reduction potential).....eqn. 3

By subtracting eqn. 3 from 1 we get,

$$*2(\text{Ir}^{\text{III}}) - 2(\text{Ir}^{\text{IV}}) - e \rightarrow 0 \text{ or, } *E^{\text{ox}} (\text{V vs SCE}) = (2.366 - 1.06) \text{ V vs SCE} = 1.306 \text{ V vs SCE}$$

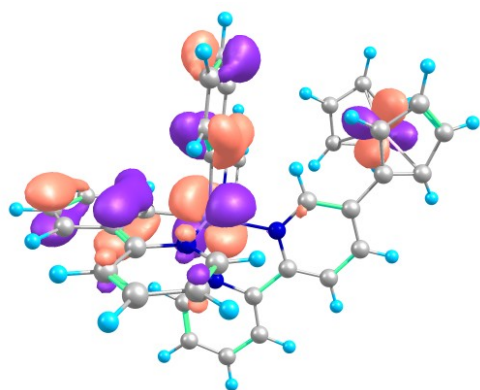
Or,

$$*2(\text{Ir}^{\text{III}}) \rightarrow 2(\text{Ir}^{\text{IV}}) + e \text{ or, } *E^{\text{ox}} (\text{V vs SCE}) = (2.366 - 1.06) \text{ V vs SCE} = 1.306 \text{ V vs SCE}$$

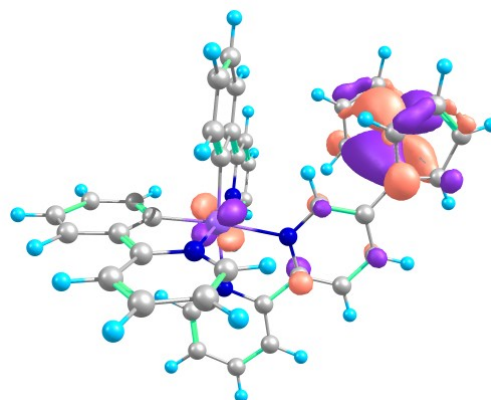
Hence, the complex **2** has excited state oxidation potential, $*E_{1/2}^{\text{ox}}$ of 1.306 V vs SCE for $*2(\text{Ir}^{\text{III}})$ to $2(\text{Ir}^{\text{IV}})$ process.

Table S3. TDDFT data of complex **2** calculated at B3LYP/B1 level of theory using acetonitrile as implicit solvent. B1 refers to a basis set where ZORA-Def2-TZVP is used for all the atoms except Ir for which SARC-ZORA-TZVP basis set is used.

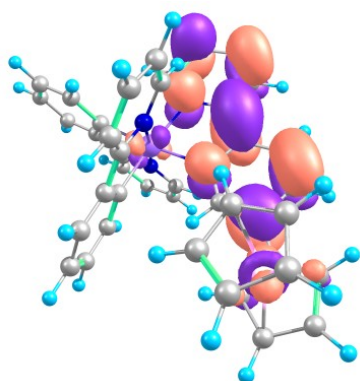
Transition Wavelength(nm)	Oscillator Strength	Excitations	Nature
265	0.187	π (ppy) \rightarrow π^* (ppy) $5d_{yz}$ (Ir) \rightarrow π^* (ppy)	Combination of ILCT on ppy ligand and MLCT
270	0.212	π (ppy), $5d_{xy}$ (Ir) \rightarrow π^* (bpy) π (ppy), $5d_{yz}$ (Ir) \rightarrow π^* (ppy)	Combination of LLCT and ILCT on ppy ligand
337	0.263	$3d_{z2}$ (Fe), π (bpy) \rightarrow π^* (bpy)	ILCT on fcbpy ligand
403	0.066	$5d_{xz}$ (Ir), π (ppy) \rightarrow π^* (ppy) $3d_{xy}$ (Fe) \rightarrow π^* (ppy)	Combination of MLCT and LLCT
434	0.036	$3d_{xy}$ (Fe), $3d_{x2-y2}$ (Fe) \rightarrow π^* (bpy)	ILCT on fcbpy ligand
487	0.010	$3d_{x2-y2}$ (Fe) \rightarrow [$3d_{xz}$ (Fe) – π (fc)] $3d_{z2}$ (Fe) \rightarrow [$3d_{yz}$ (Fe) – π (fc)]	d-d transition
557	0.020	$3d_{x2-y2}$ (Fe) \rightarrow [$3d_{xz}$ (Fe) – π (fc)] $3d_{xy}$ (Fe) \rightarrow [$3d_{yz}$ (Fe) – π (fc)]	d-d transition



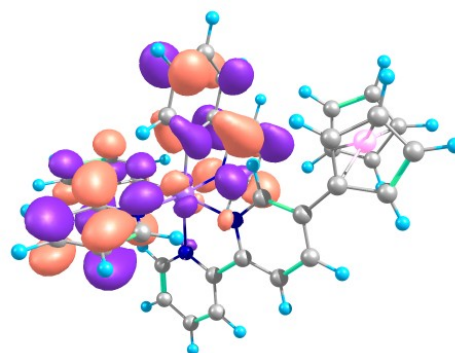
HOMO-1



HOMO



LUMO



LUMO+1

Figure S15. Frontier Orbitals of Complex 2.

7. Details of the light source used in the photocatalysis

Light Source: CFL lamp

Light colour: White

Brand: Bajaj ECOLUX

Shape: U shaped

Base Type: B-22

Power: 36 W

Material: Glass

Lumen: 2160

Temperature: 6500K

Voltage: 220-240 V

Frequency: 50 Hz

Country of origin: India

LED Lamp Specification

Light Source: LED lamp

Light colour: White

Brand: Wipro

Shape: Bulb shaped

Base Type: B-22

Power: 15 W

Material: Glass

Lumen: 1500

Temperature: 6500 K

Voltage: 220-240 V

Frequency: 50 Hz

Country of origin: India

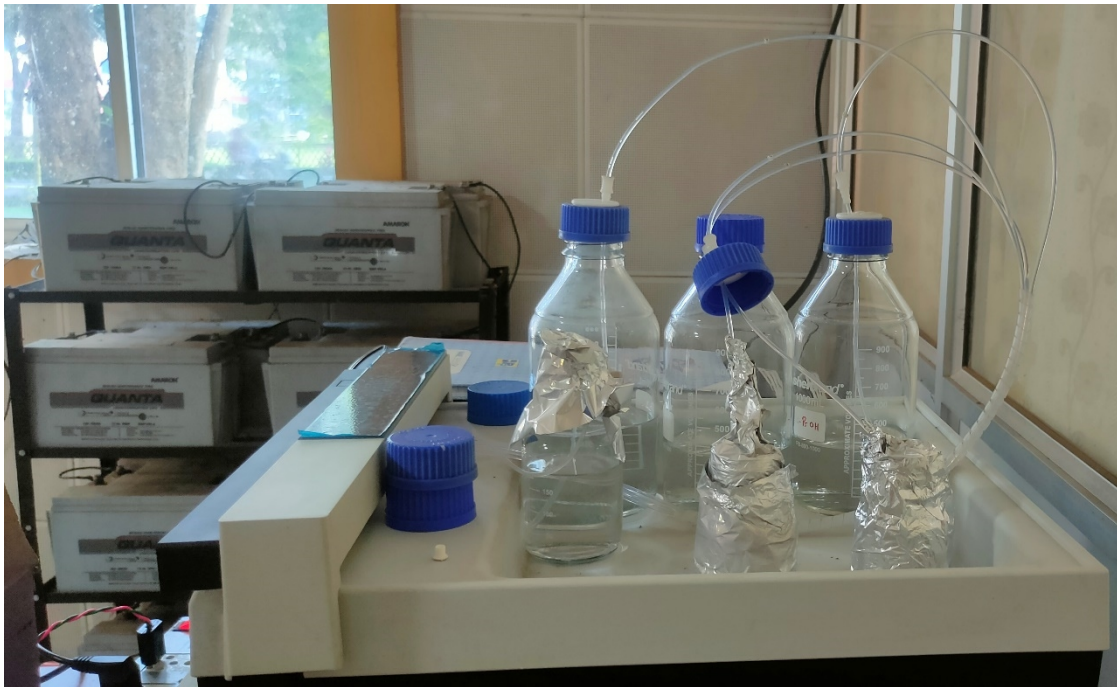
Details of Continuous Flow Microreactor Set-up:

Details of HPLC Pump: Thermo Fischer Scientific Dionex UltiMate 3000 pumps

Details of tubing: FluorothermTM Perfluoroalkoxy (PFA) tubing (Length: 15 m; Inner Diameter: 0.78 mm; Volume: 7.16 mL)

Details of the glass column: Outer diameter 12 cm.

A continuous flow photochemical microreactor was set up by wrapping a visible light transparent perfluoroalkoxy (PFA) tubing (Length: 15 m; Inner Diameter: 0.78 mm; Volume: 7.16 mL) over a borosilicate glass column (Outer Diameter: 12 cm). A 15 W white LED bulb (Outer diameter: 6 cm) was kept inside the glass column as the light source and connections were made through two high performance liquid chromatography (HPLC) pump as shown in Figure S16. In order to avoid any heating of the reaction mixture, an electric fan was continuously run throughout the experiments over the reaction set-up.



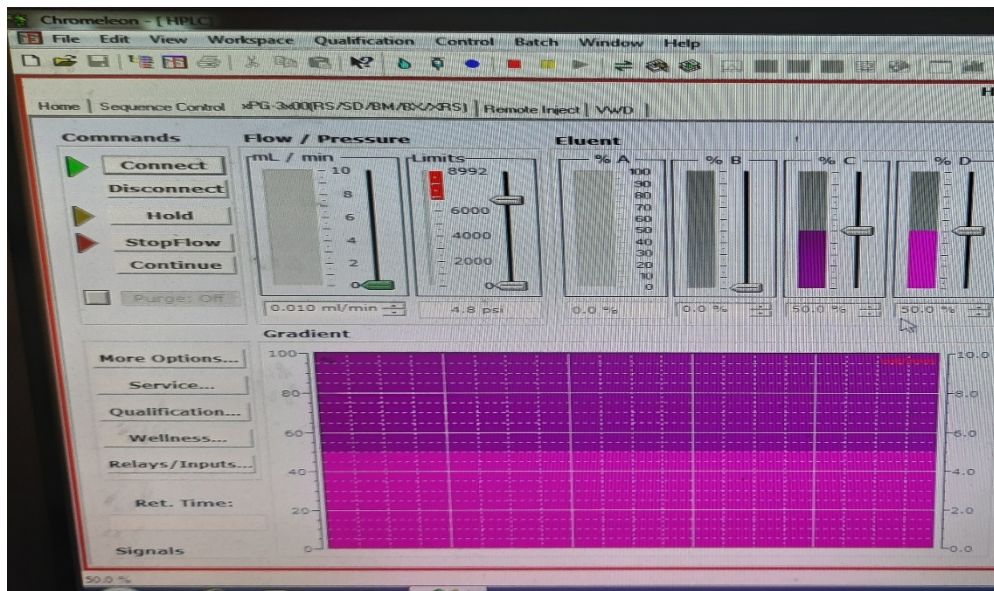
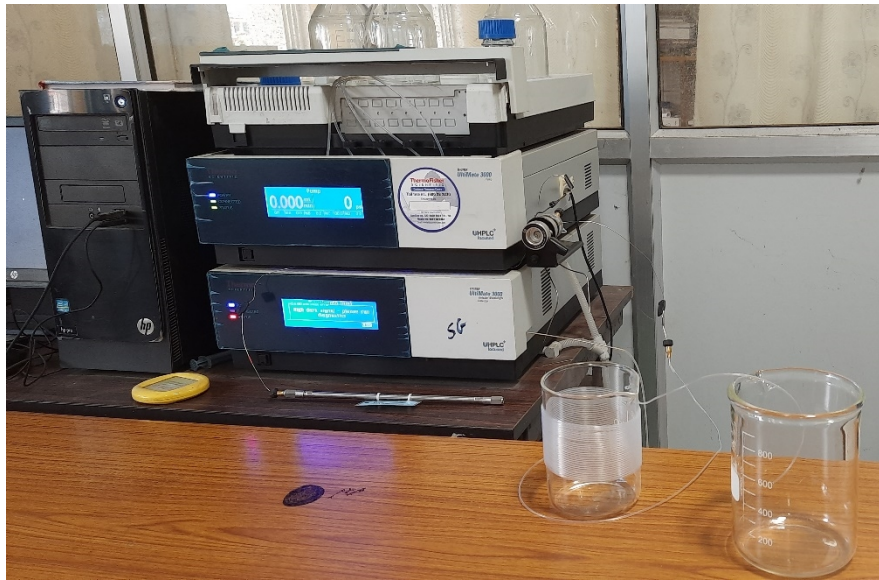




Figure S16. Photograph of the continuous flow microreactor reaction set-up

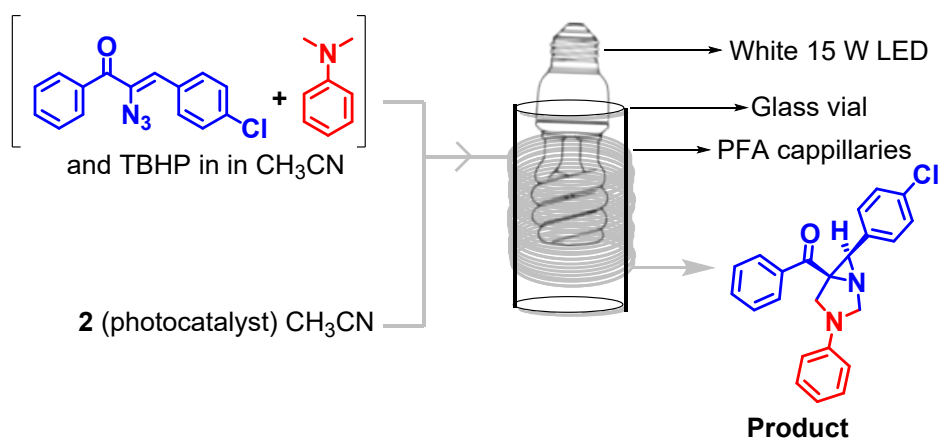
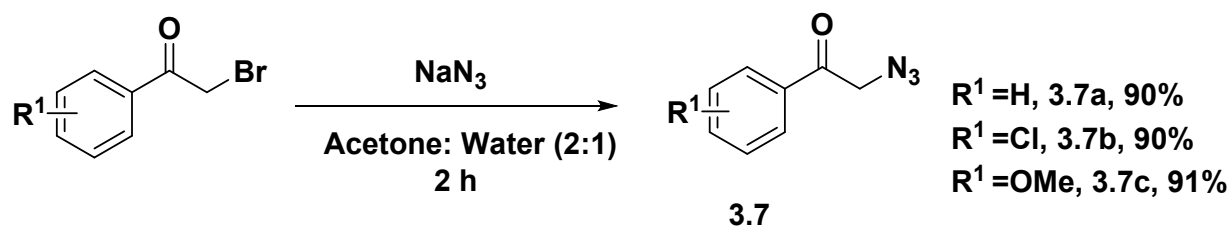


Figure 16A. Photocatalysis by **2** at continuous flow microreactor

8. General procedure for the synthesis of phenacyl azides (3.7)

The phenacyl azides were prepared from phenacyl bromides and sodium azide using literature methods.⁶

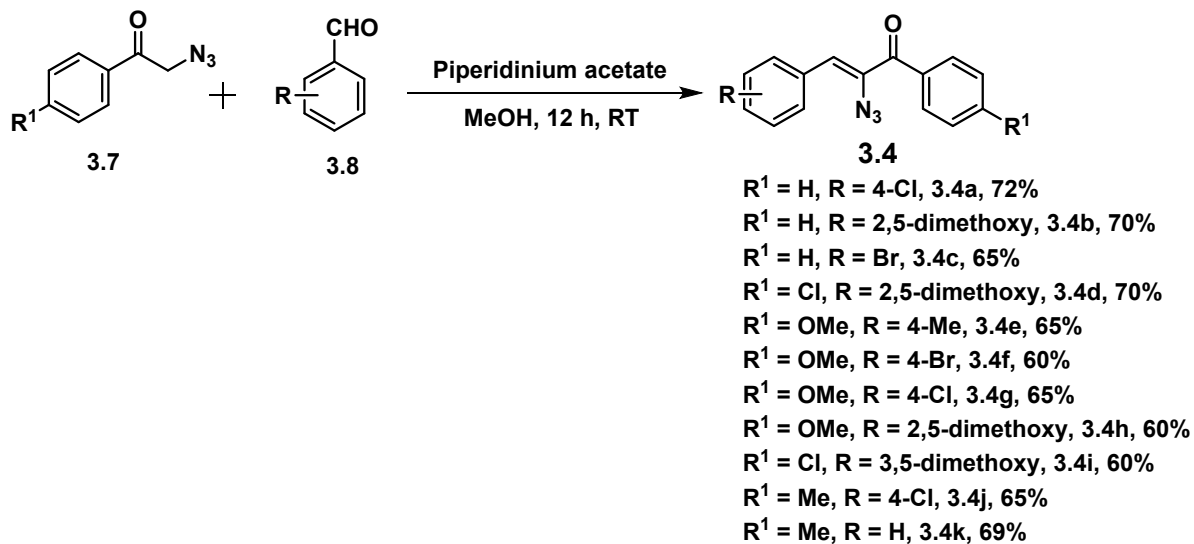


Scheme S2. Synthesis of phenacyl azides 3.7

9. Handling of azides

Organic azides are potentially shock sensitive and explosive compounds which decompose with slightest input of energy.⁷ They should be handled with care and should not be heated too much while concentrating on rotary evaporator. All the synthesized vinyl azides should be stored at low temperature and in dark.

10. General procedure for the synthesis of α -keto vinyl azides(3.4)

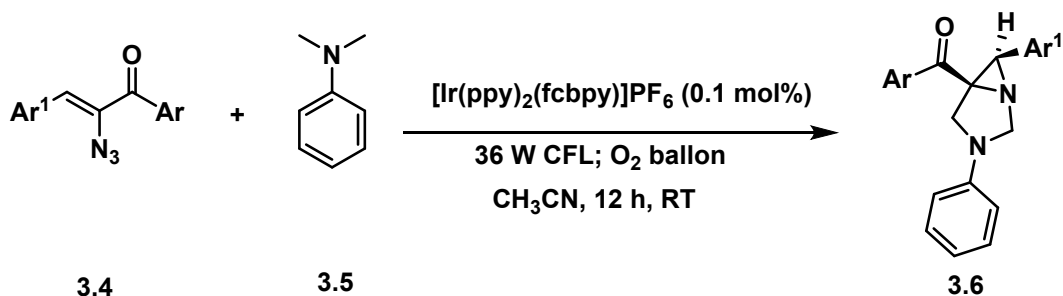


Scheme S3. Synthesis of α -keto vinyl azides 3.4

In a 25 mL round bottom flask, substituted benzaldehydes **3.8** (1 mmol) and phenacyl azides **3.7** (1 mmol) were taken to which piperidinium acetate (5 mmol) and MeOH (10 mL) was added and the reaction mixture was stirred in dark for 12 h at ambient temperature. Next, the reaction mixture was evaporated to dryness under reduced pressure using a rotary evaporator and the residue was extracted with ethyl acetate/water. The organic layer was separated, dried over anhydrous sodium sulphate, and concentrated to yield a crude product which was purified using silica-gel column chromatography to yield α -keto vinyl azides **3.4**.

11. General procedure for the synthesis of (3,6-diphenyl-1,3-diazabicyclo[3.1.0]hexan-5-yl)(phenyl)methanones (3.6a-1)

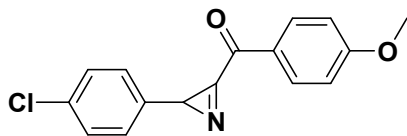
A) Batch Synthesis: In a 25 mL round bottom flask, α -ketovinylazide **3.4** (0.22 mmol) was taken in MeCN (3 mL) to which *N,N*-dimethylaniline **3.5** (0.2 mmol) was added. To this, a solution of $[\text{Ir}(\text{ppy})_2(\text{fcbpy})]\text{PF}_6$ (0.1 mol%) **2** in MeCN was added under stirring and the reaction vessel was kept under oxygen atmosphere. The vessel was then placed at a distance of 10 cm (approx.) from a white light source (36 W CFL). The reaction was monitored until its completion (TLC). Next, the reaction mixture was concentrated to give a crude product which was purified by silica-gel column chromatography using ethyl acetate/hexane in increasing polarity to yield the products **3.6**.



Scheme S4. Photochemical coupling of **3.4** and **3.5** to yield **3.6** in presence of ferrocenyl iridium(III) complex as catalyst

B) Continuous Flow Synthesis: A solution of *N,N*-dimethylanilines **3.5** and α -ketovinylazide **3.4** (0.1M in MeCN containing 5 eq. TBHP) was kept in one reservoir and a solution of photocatalyst **2** (0.1 mM in MeCN) in other one. Both the solutions were pumped and mixed through a T-junction using two HPLC pumps at the same flow rates. Under stable conditions, the reaction mixture (10 mL) from the microreactor outlet was collected and concentrated to yield a crude product which was purified by silica-gel column chromatography to yield compounds **3.6** in pure forms.

12A. Characterization of (2-(4-chlorophenyl)-2H-azirin-3-yl)(4-methoxyphenyl)methanone



^1H NMR (400 MHz, Chloroform-*d*) δ 8.27 (d, $J = 9.0$ Hz, 2H), 7.29 (d, $J = 8.5$ Hz, 2H), 7.12 (d, $J = 8.5$ Hz, 2H), 7.04 (d, $J = 8.9$ Hz, 2H), 3.93 (s, 3 H), 3.44 (s, 1H). ^{13}C {1H} NMR (101 MHz, Chloroform-*d*) δ 180.4, 165.9, 165.1, 137.8, 133.8, 132.4, 128.8, 127.8, 114.8, 55.9, 36.9, 29.8.

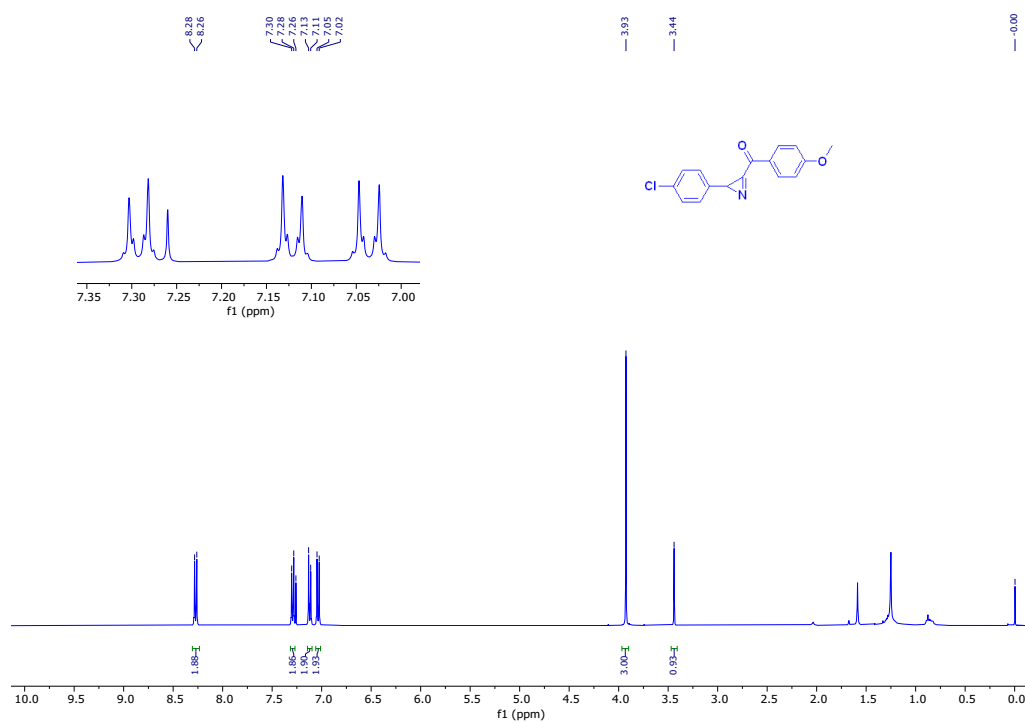


Figure S17. ^1H NMR spectrum (400 MHz, CDCl_3)

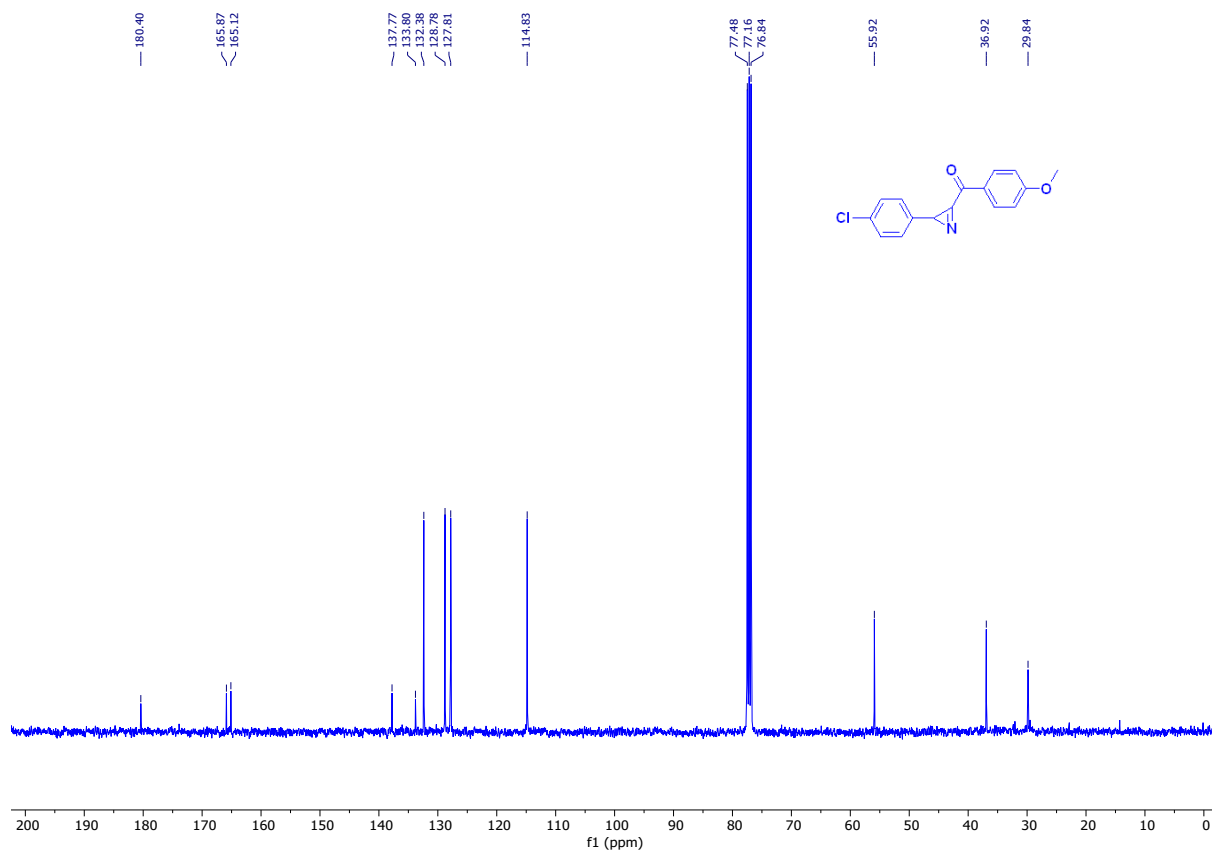
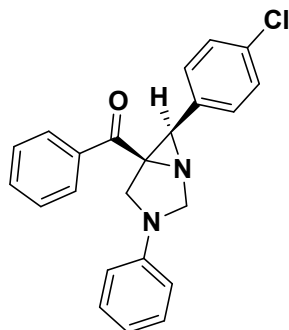


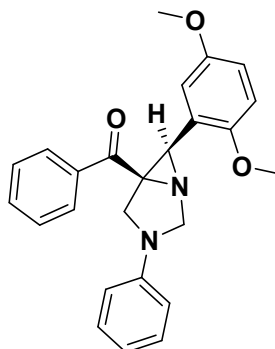
Figure S18. ^{13}C NMR Spectrum (101 MHz, CDCl_3)

12B.Characterization of (6-(4-chlorophenyl)-3-phenyl-1,3-diazabicyclo[3.1.0]hexan-5-yl)(phenyl)methanone(3.6a)



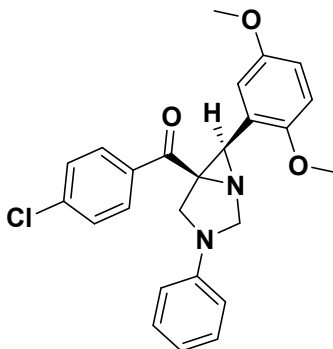
Prepared following the general procedure 11B; white solid; yield 176 mg, 94%; $R_f = 0.53$ (EtOAc/Hexane = 1/10); mp 189-190 °C; IR (CHCl₃, cm⁻¹): 2918, 2851, 1730, 1600, 1492, 1359, 1216, 1175. ¹H NMR (500 MHz, CDCl₃) δ 7.92 (d, $J = 7.7$ Hz, 2H), 7.55 (t, $J = 7.5$ Hz, 1H), 7.42 (t, $J = 7.7$ Hz, 2H), 7.28 – 7.22 (m, 4H), 7.15 (d, $J = 8.2$ Hz, 2H), 6.82 (t, $J = 7.4$ Hz, 1H), 6.61 (d, $J = 8.1$ Hz, 2H), 4.77 (d, $J = 7.7$ Hz, 1H), 4.51 (d, $J = 7.6$ Hz, 1H), 4.37 (d, $J = 9.8$ Hz, 1H), 3.54 (s, 1H), 3.41 (d, $J = 9.8$ Hz, 1H). ¹³C NMR (125 MHz, CDCl₃) δ 193.86, 145.81, 135.95, 133.68, 133.27, 133.24, 129.39, 128.79, 128.56, 128.37, 128.32, 118.39, 113.11, 70.70, 61.46, 50.38, 47.85. HRMS (ESI, Orbitrap) calcd for C₂₃H₁₉N₂OCl [M+H]⁺ = 375.1264, found = 375.1259.

(6-(2,5-dimethoxyphenyl)-3-phenyl-1,3-diazabicyclo[3.1.0]hexan-5-yl)(phenyl)methanone
(3.6b)



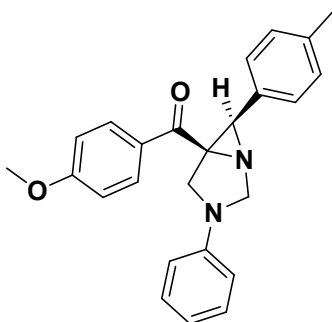
Prepared following the general procedure 11B; white solid, yield 182 mg, 91%; $R_f = 0.32$ (EtOAc/Hexane = 1/10); mp 180-181°C; IR (CHCl₃, cm⁻¹): 2918, 2850, 1678, 1600, 1498, 1361, 1218. ¹H NMR (500 MHz, CDCl₃) δ 7.99 (d, $J = 7.8$ Hz, 2H), 7.52 (t, $J = 7.5$ Hz, 1H), 7.40 (t, $J = 7.6$ Hz, 2H), 7.32 – 7.20 (m, 2H), 6.92 (s, 1H), 6.80 (t, $J = 7.4$ Hz, 1H), 6.66 – 6.60 (m, 4H), 4.70 (d, $J = 7.6$ Hz, 1H), 4.49 (d, $J = 7.5$ Hz, 1H), 4.42 (d, $J = 9.7$ Hz, 1H), 3.87 (s, 1H), 3.80 (s, 3H), 3.65 (s, 3H), 3.39 (d, $J = 9.7$ Hz, 1H). ¹³C NMR (125 MHz, CDCl₃) δ 194.20, 153.23, 151.76, 145.96, 136.44, 133.26, 129.33, 128.80, 128.27, 123.46, 117.99, 114.14, 112.93, 112.61, 110.84, 70.67, 61.34, 55.59, 55.57, 50.09, 45.02. HRMS (ESI, Orbitrap) calcd for C₂₅H₂₄N₂O₃ [M+H]⁺ = 401.1865, found = 401.1863.

(4-chlorophenyl)(6-(2,5-dimethoxyphenyl)-3-phenyl-1,3-diazabicyclo[3.1.0]hexan-5-yl)methanone (3.6c)



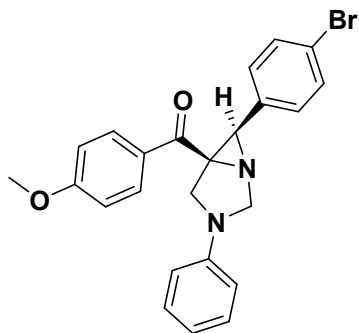
Prepared following the general procedure 11B; white solid; yield 200 mg, 92%; $R_f = 0.35$ (EtOAc/Hexane = 1/10); mp 182-183 °C; IR (CHCl₃, cm⁻¹): 2919, 2851, 1737, 1600, 1466, 1216, 1118. ¹H NMR (500 MHz, CDCl₃) δ 7.93 (d, $J = 7.3$ Hz, 2H), 7.36 (d, $J = 6.3$ Hz, 2H), 7.27 (m, 3H), 6.90 (s, 1H), 6.82 (d, $J = 8.6$ Hz, 1H), 6.66 – 6.58 (m, 3H), 4.70 (d, $J = 5.8$ Hz, 1H), 4.48 (d, $J = 6.7$ Hz, 1H), 4.39 (d, $J = 9.7$ Hz, 1H), 3.85 (d, $J = 3.2$ Hz, 1H), 3.80 (s, 3H), 3.66 (s, 3H), 3.38 (d, $J = 8.6$ Hz, 1H). ¹³C NMR (125 MHz, CDCl₃) δ 193.27, 153.26, 151.67, 145.87, 139.72, 134.70, 130.22, 129.35, 128.57, 123.25, 118.12, 114.07, 112.95, 112.78, 110.86, 70.65, 61.09, 55.61, 55.57, 49.91, 44.99. HRMS (ESI, Orbitrap) calcd for C₂₅H₂₃N₂O₃Cl [M+H]⁺ = 435.1475, found = 435.1477.

(4-methoxyphenyl)(3-phenyl-6-(p-tolyl)-1,3-diazabicyclo[3.1.0]hexan-5-yl)methanone (3.6d)



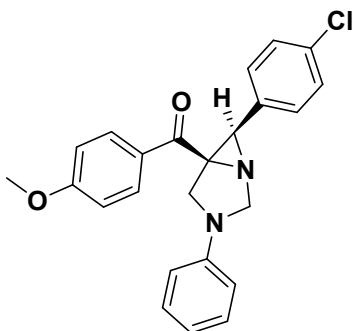
Prepared following the general procedure 11B; white solid; yield 183 mg, 95%; $R_f = 0.29$ (EtOAc/Hexane = 1/10); mp 173-175 °C; IR (CHCl₃, cm⁻¹): 2919, 2851, 1673, 1600, 1508, 1362, 1262, 1163. ¹H NMR (500 MHz, CDCl₃) δ 8.00 – 7.95 (m, 2H), 7.28 – 7.25 (m, 2H), 7.17 – 7.15 (m, 2H), 6.99 (d, $J = 7.9$ Hz, 2H), 6.91 – 6.86 (m, 2H), 6.83-6.79 (m, 1H), 6.60 (d, $J = 7.6$ Hz, 2H), 4.75 (d, $J = 7.6$ Hz, 1H), 4.51 (d, $J = 7.6$ Hz, 1H), 4.34 (d, $J = 9.7$ Hz, 1H), 3.85 (s, 3H), 3.48 (s, 1H), 3.39 (d, $J = 9.7$ Hz, 1H), 2.22 (s, 3H). ¹³C NMR (125 MHz, CDCl₃) δ 192.43, 163.79, 145.98, 137.02, 131.85, 131.34, 129.36, 129.03, 128.86, 126.79, 118.12, 113.71, 113.02, 70.84, 61.31, 55.40, 50.72, 48.41, 20.99. HRMS (ESI, Orbitrap) calcd for C₂₅H₂₄N₂O₂[M+H]⁺ = 385.1916, found = 385.1913.

**(6-(4-bromophenyl)-3-phenyl-1,3-diazabicyclo[3.1.0]hexan-5-yl)(4-methoxyphenyl)methanone
(36e)**



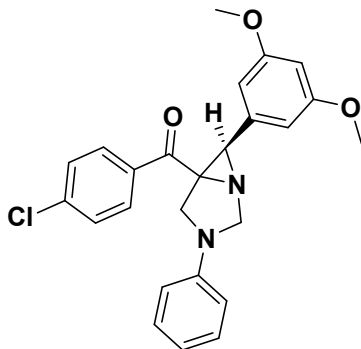
Prepared following the general procedure 11B; white solid; yield 209 mg, 93%; $R_f = 0.35$ (EtOAc/Hexane = 1/10); mp 183-185 °C; IR (CHCl₃, cm⁻¹): 2918, 2850, 1671, 1599, 1507, 1359, 1262, 1163. ¹H NMR (500 MHz, CDCl₃) δ 7.96 – 7.92 (m, 2H), 7.32 – 7.27 (m, 3H), 7.23 (s, 1H), 7.16 – 7.12 (m, 2H), 6.91 – 6.77 (m, 3H), 6.61 – 6.58 (m, 2H), 4.74 (d, $J = 7.6$ Hz, 1H), 4.49 (d, $J = 7.6$ Hz, 1H), 4.34 (d, $J = 9.8$ Hz, 1H), 3.85 (s, 3H), 3.45 (s, 1H), 3.38 (d, $J = 9.8$ Hz, 1H). ¹³C NMR (125 MHz, CDCl₃) δ 191.72, 164.31, 146.07, 134.30, 133.88, 131.51, 131.44, 129.59, 128.85, 121.53, 118.53, 114.01, 113.30, 70.93, 61.50, 55.63, 50.83, 47.79. HRMS (ESI, Orbitrap) calcd for C₂₄H₂₁N₂O₂Br [M+H]⁺ = 449.0865, found = 449.0869.

**(6-(4-chlorophenyl)-3-phenyl-1,3-diazabicyclo[3.1.0]hexan-5-yl)(4-methoxyphenyl)methanone
(3.6f)**



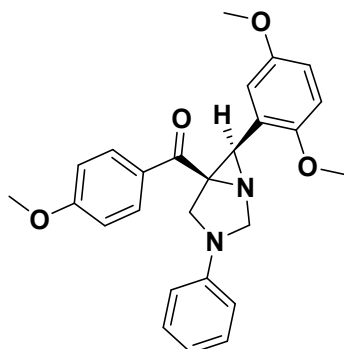
Prepared following the general procedure 11B; white solid; yield 182 mg, 90%; $R_f = 0.35$ (EtOAc/Hexane = 1/10); mp 185-186 °C; IR (CHCl₃, cm⁻¹): 2916, 2849, 1675, 1600, 1505, 1360, 1245, 1164. ¹H NMR (500 MHz, CDCl₃) δ 8.03 – 7.91 (m, 2H), 7.29 – 7.09 (m, 6H), 6.89 – 6.77 (m, 3H), 6.63 – 6.56 (m, 2H), 4.75 (d, $J = 7.7$ Hz, 1H), 4.49 (d, $J = 7.6$ Hz, 1H), 4.34 (d, $J = 9.8$ Hz, 1H), 3.84 (s, 3H), 3.47 (s, 1H), 3.39 (d, $J = 9.8$ Hz, 1H). ¹³C NMR (125 MHz, CDCl₃) δ 192.24, 164.18, 146.09, 133.77, 133.38, 131.50, 129.59, 129.04, 128.50, 124.10, 118.52, 114.00, 113.30, 70.94, 61.52, 55.61, 50.83, 47.74. HRMS (ESI, Orbitrap) calcd for C₂₄H₂₁N₂O₂Cl [M+H]⁺ = 405.1370, found = 405.1374.

(4-chlorophenyl)(6-(3,5-dimethoxyphenyl)-3-phenyl-1,3-diazabicyclo[3.1.0]hexan-5-yl)methanone
(3.6g)



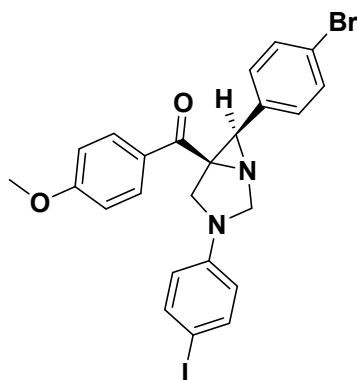
Prepared following the general procedure 11B; white solid; yield 202 mg, 93%; $R_f = 0.34$ (EtOAc/Hexane = 1/10); mp 142-144 °C; IR (CHCl₃, cm⁻¹): 2922, 2855, 1704, 1606, 1460, 1353, 1249, 1160. ¹H NMR (500 MHz, CDCl₃) δ 7.93 (d, $J = 19.6$ Hz, 2H), 7.38 (s, 2H), 6.90 – 6.07 (m, 8H), 4.75 (s, 1H), 4.50 (s, 1H), 4.34 (s, 1H), 3.64 (s, 6H), 3.48 (s, 1H), 3.38 (s, 1H). ¹³C NMR (125 MHz, CDCl₃) δ 193.67, 160.76, 146.07, 140.22, 137.07, 134.82, 130.53, 129.64, 129.00, 118.64, 113.36, 105.06, 100.36, 71.02, 61.37, 55.37, 50.48, 48.93. HRMS (ESI, Orbitrap) calcd for C₂₅H₂₃ClN₂O₃ [M+H]⁺ = 434.1397, found = 434.1392.

**(6-(2,5-dimethoxyphenyl)-3-phenyl-1,3-diazabicyclo[3.1.0]hexan-5-yl)(4-methoxyphenyl)
methanone (3.6h)**



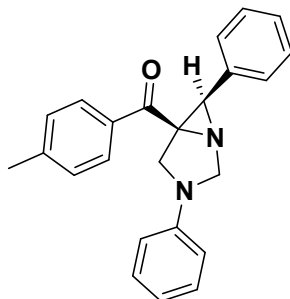
Prepared following the general procedure 11B; white solid; yield 202 mg, 94%; $R_f = 0.35$ (EtOAc/Hexane = 1/10); mp 170-172 °C; IR (CHCl₃, cm⁻¹): 2925, 2851, 1673, 1600, 1496, 1270, 1161. ¹H NMR (500 MHz, CDCl₃) δ 8.00 (d, $J = 8.5$ Hz, 2H), 7.25 (d, $J = 3.2$ Hz, 2H), 6.93 – 6.74 (m, 4H), 6.61 (dt, $J = 11.1, 8.3$ Hz, 4H), 4.68 (d, $J = 7.5$ Hz, 1H), 4.48 (d, $J = 7.5$ Hz, 1H), 4.38 (d, $J = 9.7$ Hz, 1H), 3.83 (d, $J = 3.2$ Hz, 4H), 3.79 (s, 3H), 3.64 (s, 3H), 3.37 (d, $J = 9.6$ Hz, 1H). ¹³C NMR (125 MHz, CDCl₃) δ 192.59, 163.91, 153.55, 152.05, 146.27, 131.49, 129.56, 124.10, 118.17, 114.29, 113.73, 113.17, 112.72, 111.18, 71.00, 61.49, 55.92, 55.83, 55.61, 50.65, 44.82. HRMS (ESI, Orbitrap) calcd for C₂₆H₂₆N₂O₄ [M+H]⁺ = 431.1971, found = 431.1967.

**(6-(4-bromophenyl)-3-(4-iodophenyl)-1,3-diazabicyclo[3.1.0]hexan-5-yl)(4-methoxyphenyl)
methanone (3.6i)**



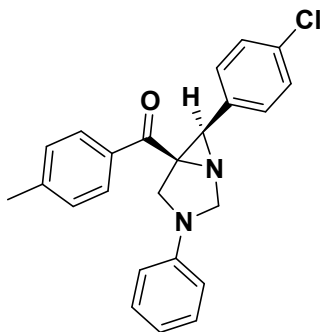
Prepared following the general procedure 11B; white solid; yield 262 mg, 91%; $R_f = 0.35$ (EtOAc/Hexane = 1/10); mp 197-199 °C; IR (CHCl₃, cm⁻¹): 2916, 2849, 1669, 1599, 1505, 1261, 1167. ¹H NMR (500 MHz, CDCl₃) δ 7.94 – 7.88 (m, 2H), 7.52 – 7.45 (m, 2H), 7.32 – 7.23 (m, 2H), 7.17 – 7.08 (m, 2H), 6.91 – 6.77 (m, 2H), 6.39 – 6.32 (m, 2H), 4.69 (d, $J = 7.8$ Hz, 1H), 4.47 (d, $J = 7.6$ Hz, 1H), 4.29 (d, $J = 9.9$ Hz, 1H), 3.84 (s, 3H), 3.40 (s, 1H), 3.36 (d, $J = 9.8$ Hz, 1H). ¹³C NMR (125 MHz, CDCl₃) δ 191.35, 173.77, 164.24, 145.58, 138.12, 134.03, 131.48, 128.82, 121.70, 115.47, 114.05, 80.77, 70.89, 61.46, 55.64, 50.77, 48.04. HRMS (ESI, Orbitrap) calcd for C₂₄H₂₀N₂O₂BrI [M+H]⁺ = 574.9817, found = 574.9827.

[1,1'-biphenyl]-4-yl((5R,6R)-6-(4-chlorophenyl)-3-phenyl-1,3-diazabicyclo[3.1.0]hexan-5-yl)methanone (3.6j)



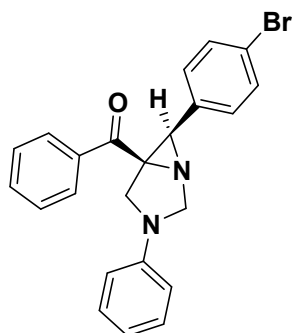
Prepared following the general procedure 11B; white solid; yield 159 mg, 90%; $R_f = 0.29$ (EtOAc/Hexane = 1/10); mp 166-168 °C; IR (CHCl₃, cm⁻¹): IR (CHCl₃, cm⁻¹): 2964, 2918, 2850, 1675, 1600, 1504, 1263, 1158. ¹H NMR (500 MHz, CDCl₃) δ 7.84 (d, $J = 7.9$ Hz, 2H), 7.41 – 7.08 (m, 9H), 6.80 (t, $J = 7.4$ Hz, 1H), 6.59 (d, $J = 8.0$ Hz, 2H), 4.75 (d, $J = 7.6$ Hz, 1H), 4.51 (d, $J = 7.6$ Hz, 1H), 4.35 (d, $J = 9.8$ Hz, 1H), 3.53 (s, 1H), 3.38 (d, $J = 9.7$ Hz, 1H), 2.37 (s, 3H). ¹³C NMR (125 MHz, CDCl₃) δ 192.83, 146.03, 144.64, 131.04, 130.06, 129.56, 129.39, 129.20, 128.32, 127.62, 127.20, 118.40, 113.26, 71.05, 61.19, 50.83, 48.82, 21.84. HRMS (ESI, Orbitrap) calcd for C₂₄H₂₂N₂O [M+H]⁺ = 355.1805, found = 355.1811.

(6-(4-chlorophenyl)-3-phenyl-1,3-diazabicyclo[3.1.0]hexan-5-yl)(p-tolyl)methanone (3.6k)



Prepared following the general procedure 11B; white solid; yield 179 mg, 92%; $R_f = 0.53$ (EtOAc/Hexane = 1/10); mp 163-165 °C; IR (CHCl₃, cm⁻¹): 2919, 2852, 1680, 1602, 1505, 1360, 1237, 1169. ¹H NMR (500MHz, CDCl₃) δ 8.00 – 7.93 (m, 1H), 7.86 – 7.79 (m, 2H), 7.52 – 7.46 (m, 1H), 7.34 – 7.31 (m, 1H), 7.24 – 7.19 (m, 3H), 7.14 (d, $J = 8.6$ Hz, 2H), 6.81 (t, $J = 7.3$ Hz, 1H), 6.59 (d, $J = 7.7$ Hz, 2H), 4.75 (d, $J = 7.7$ Hz, 1H), 4.49 (d, $J = 7.6$ Hz, 1H), 4.35 (d, $J = 9.9$ Hz, 1H), 3.50 (s, 1H), 3.38 (d, $J = 9.8$ Hz, 1H), 2.38 (s, 3H). ¹³C NMR (125 MHz, CDCl₃) δ 193.43, 146.05, 145.02, 133.62, 131.33, 131.00, 129.59, 129.50, 129.34, 129.17, 128.54, 118.54, 113.30, 70.93, 61.69, 50.73, 47.96, 21.88. HRMS (ESI, Orbitrap) calcd for C₂₅H₂₄N₂O₂[M+H]⁺ = 389.1421, found = 389.1422.

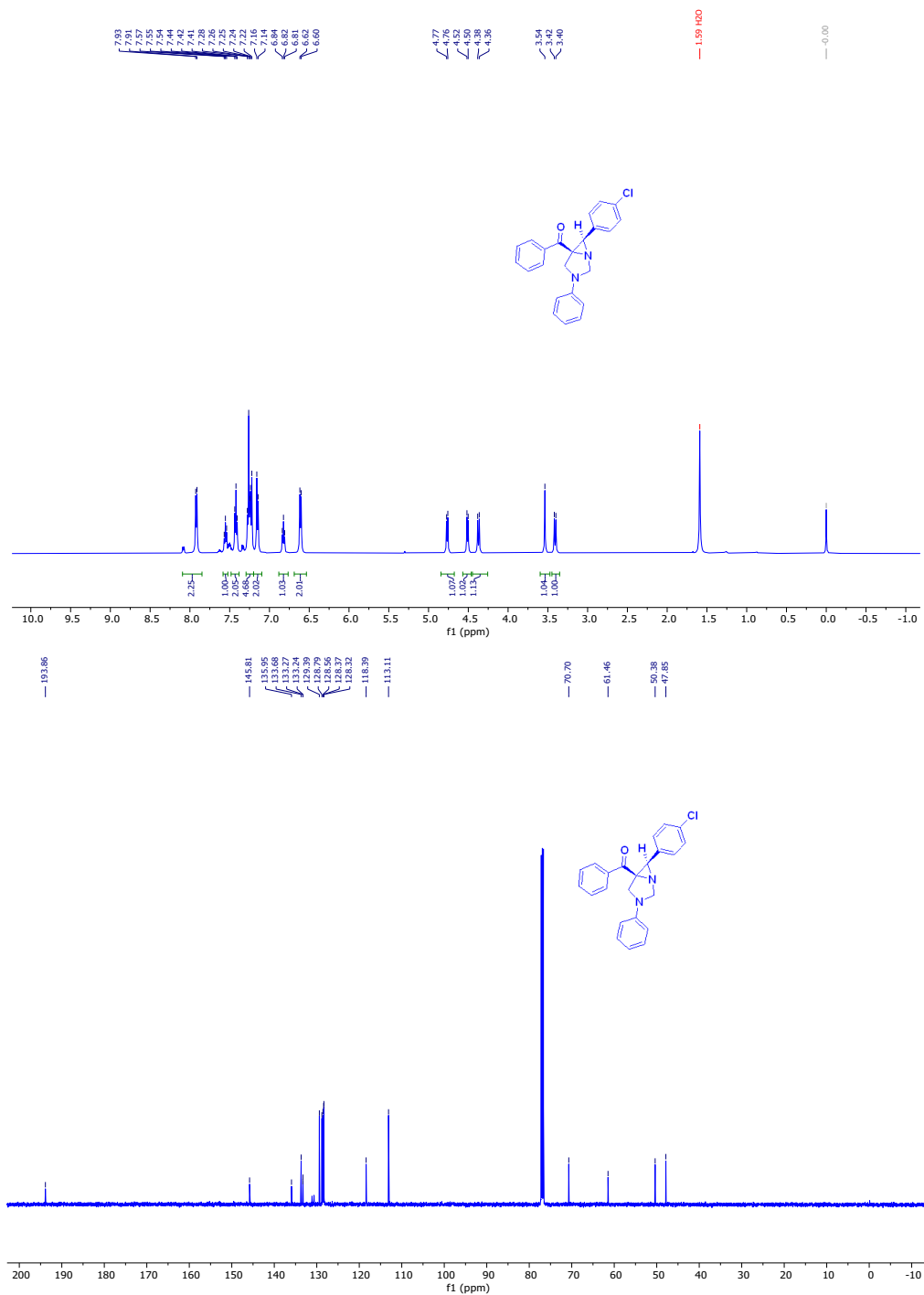
(6-(4-bromophenyl)-3-phenyl-1,3-diazabicyclo[3.1.0]hexan-5-yl)(phenyl)methanone (3.6l)



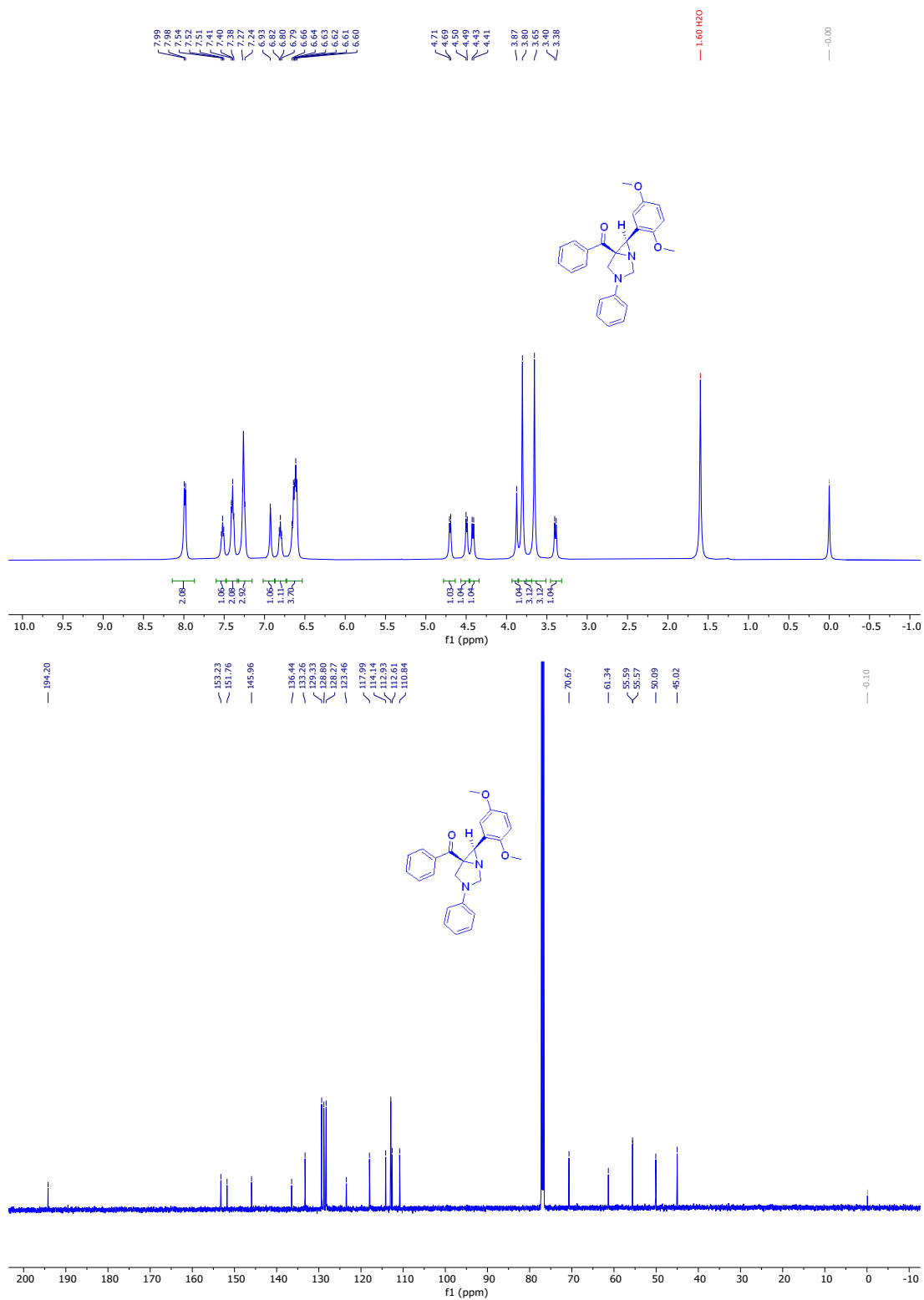
Prepared following the general procedure 11B; white solid; yield 195 mg, 93%; $R_f = 0.53$ (EtOAc/Hexane = 1/10); mp 185-187 °C; IR (CHCl₃, cm⁻¹): 2916, 2852, 1682, 1600, 1505, 1359, 1235, 1174. ¹H NMR (500 MHz, CDCl₃) δ 8.07 (dd, $J = 8.3, 1.4$ Hz, 1H), 7.91 (dd, $J = 8.3, 1.4$ Hz, 2H), 7.66 – 7.52 (m, 1H), 7.50 – 7.46 (m, 1H), 7.44 – 7.41 (m, 2H), 7.29 (dd, $J = 8.1, 6.1$ Hz, 2H), 7.17 – 7.15 (m, 2H), 6.83 – 6.79 (m, 1H), 6.61 – 6.58 (m, 2H), 4.75 (d, $J = 7.7$ Hz, 1H), 4.49 (d, $J = 7.6$ Hz, 1H), 4.36 (d, $J = 9.9$ Hz, 1H), 3.51 (s, 1H), 3.39 (d, $J = 9.8$ Hz, 1H). ¹³C NMR (125 MHz, CDCl₃) δ 193.91, 145.87, 136.03, 133.68, 133.30, 129.42, 128.83, 128.58, 128.42, 128.35, 124.21, 118.43, 113.16, 70.76, 61.50, 50.43, 47.90. HRMS (ESI, Orbitrap) calcd for C₂₃H₁₉BrN₂O [M+H]⁺ = 419.0759, found = 419.0755.

12. ^1H NMR and ^{13}C NMR Spectra of (3,6-diphenyl-1,3-diazabicyclo[3.1.0]hexan-5-yl)(phenyl)methanones

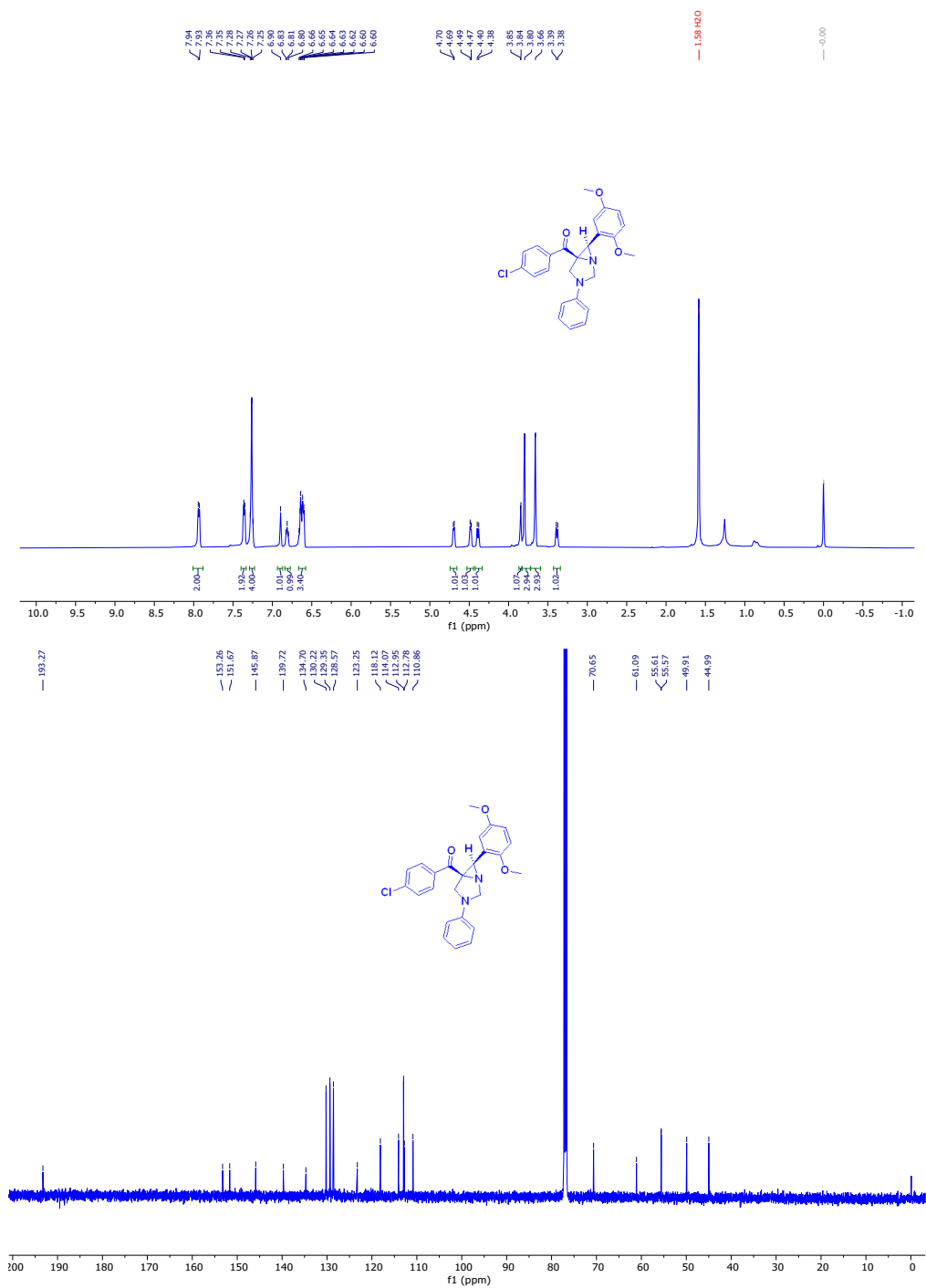
^1H NMR and ^{13}C NMR Spectra of 3.6a



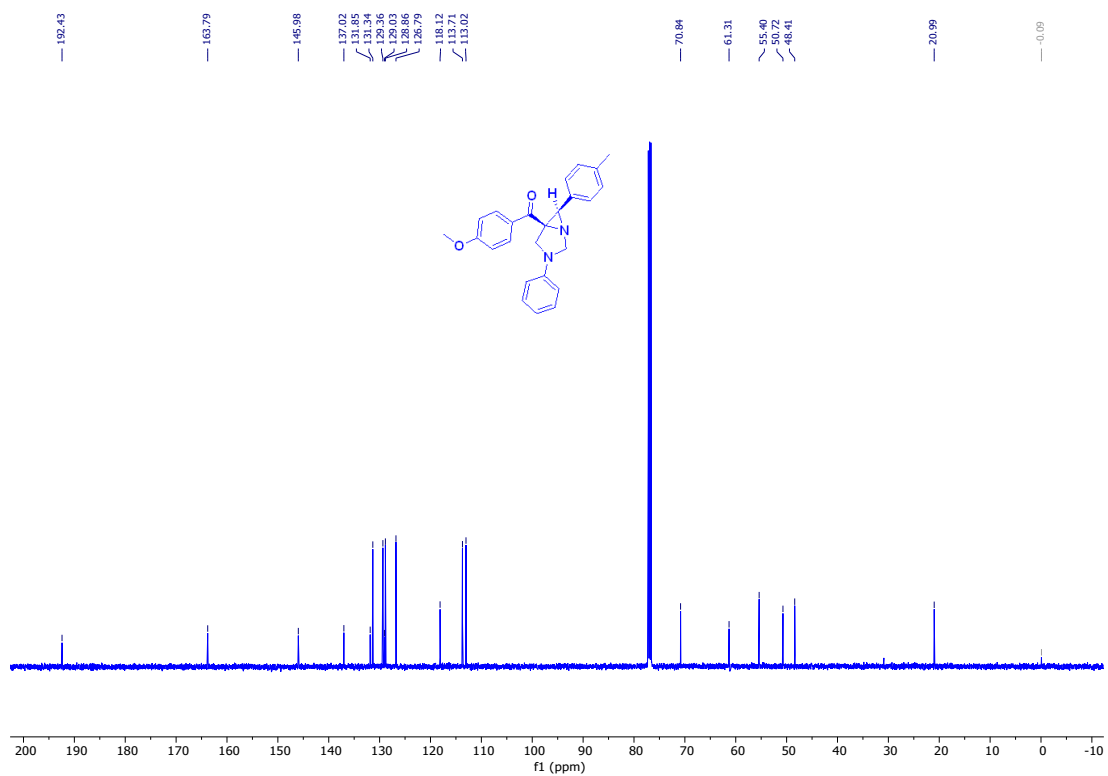
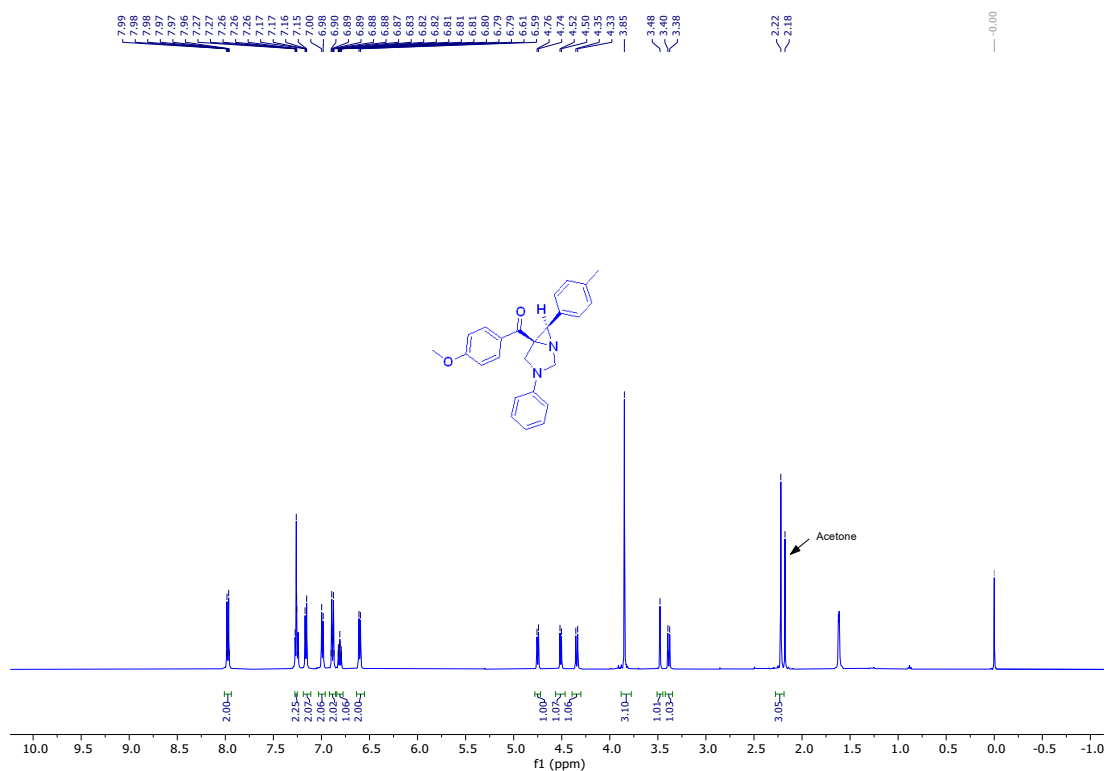
^1H NMR and ^{13}C NMR Spectra of 3.6b



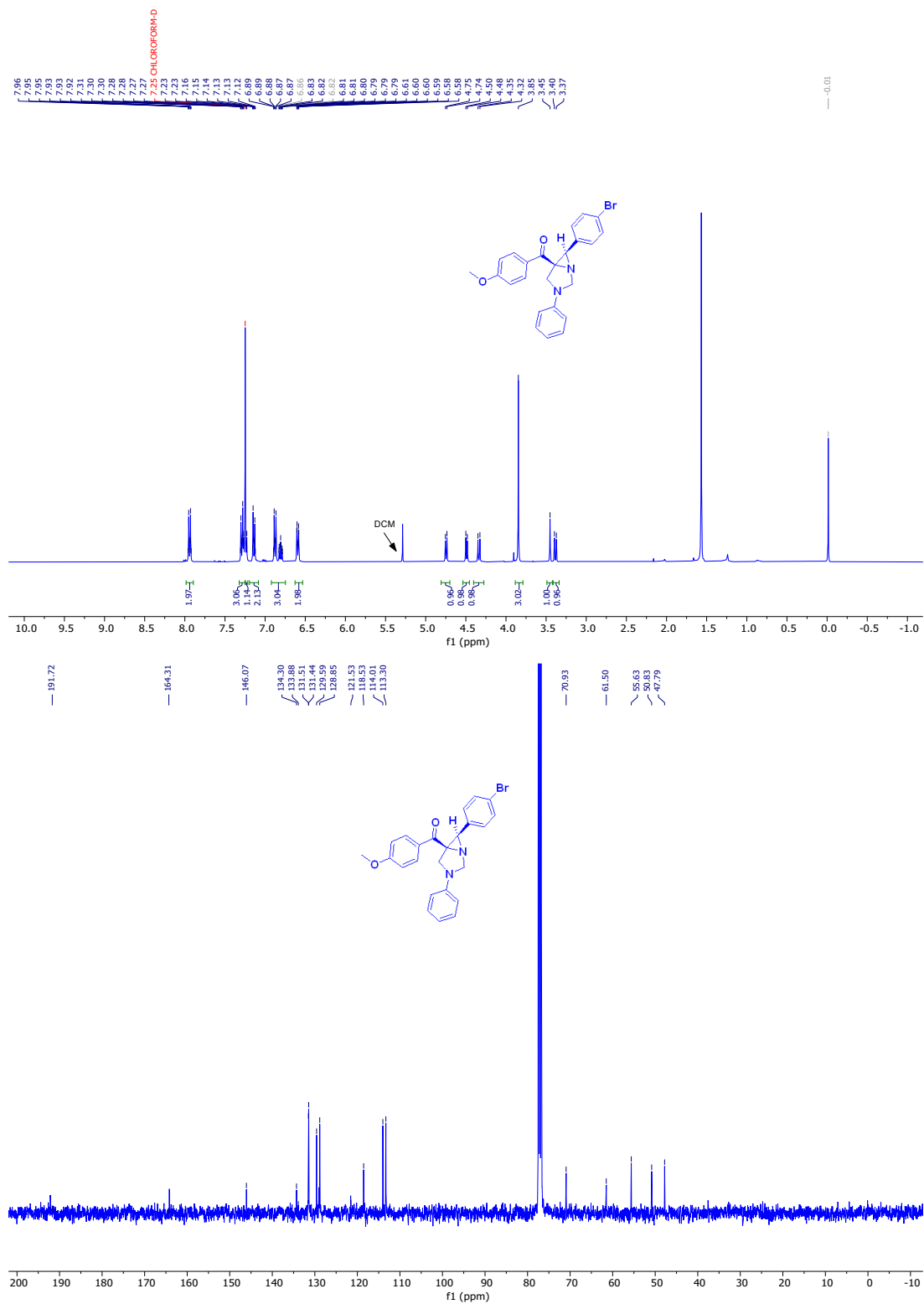
^1H NMR and ^{13}C NMR Spectra of 3.6c



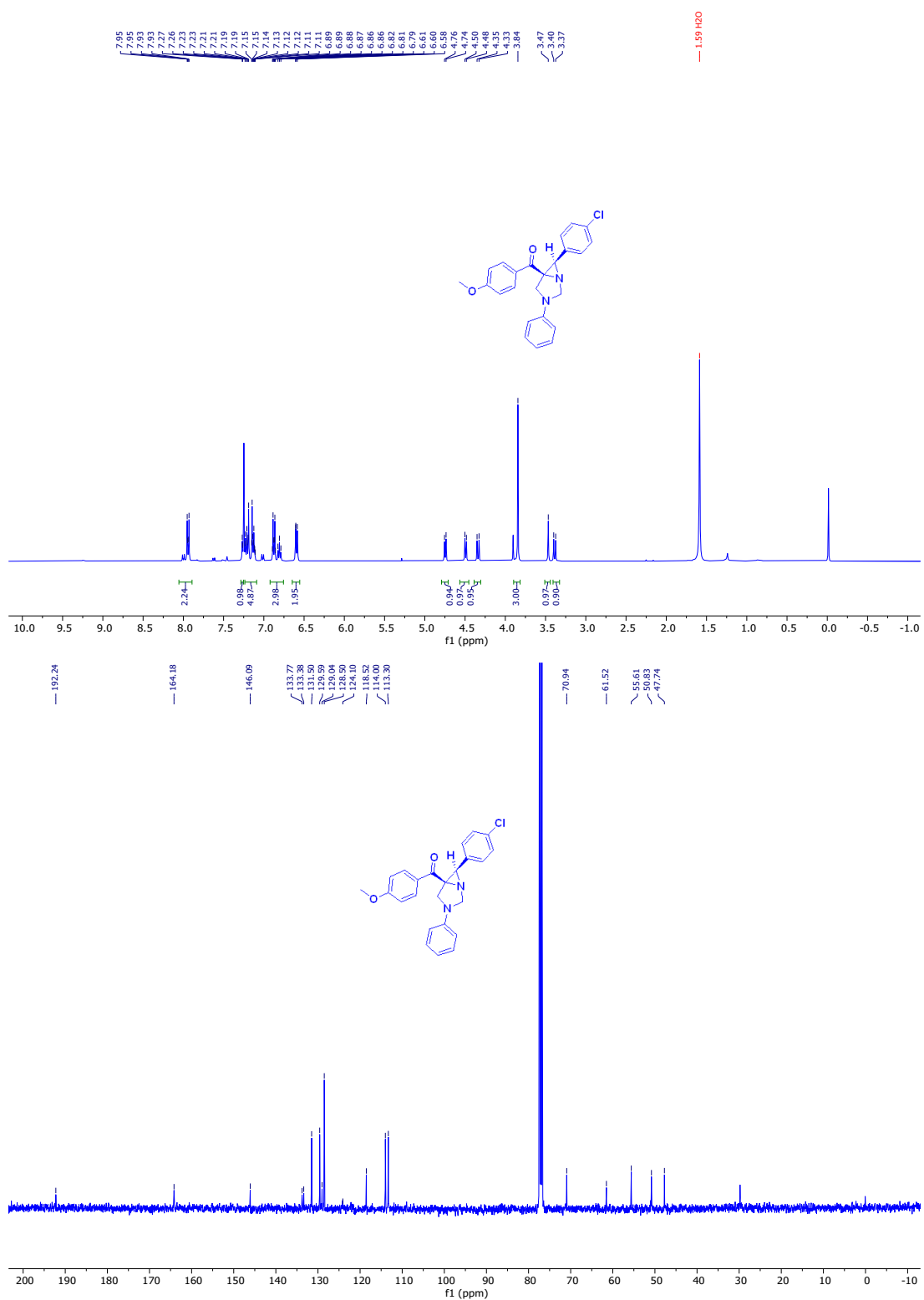
¹H NMR and ¹³C NMR Spectra of 3.6d



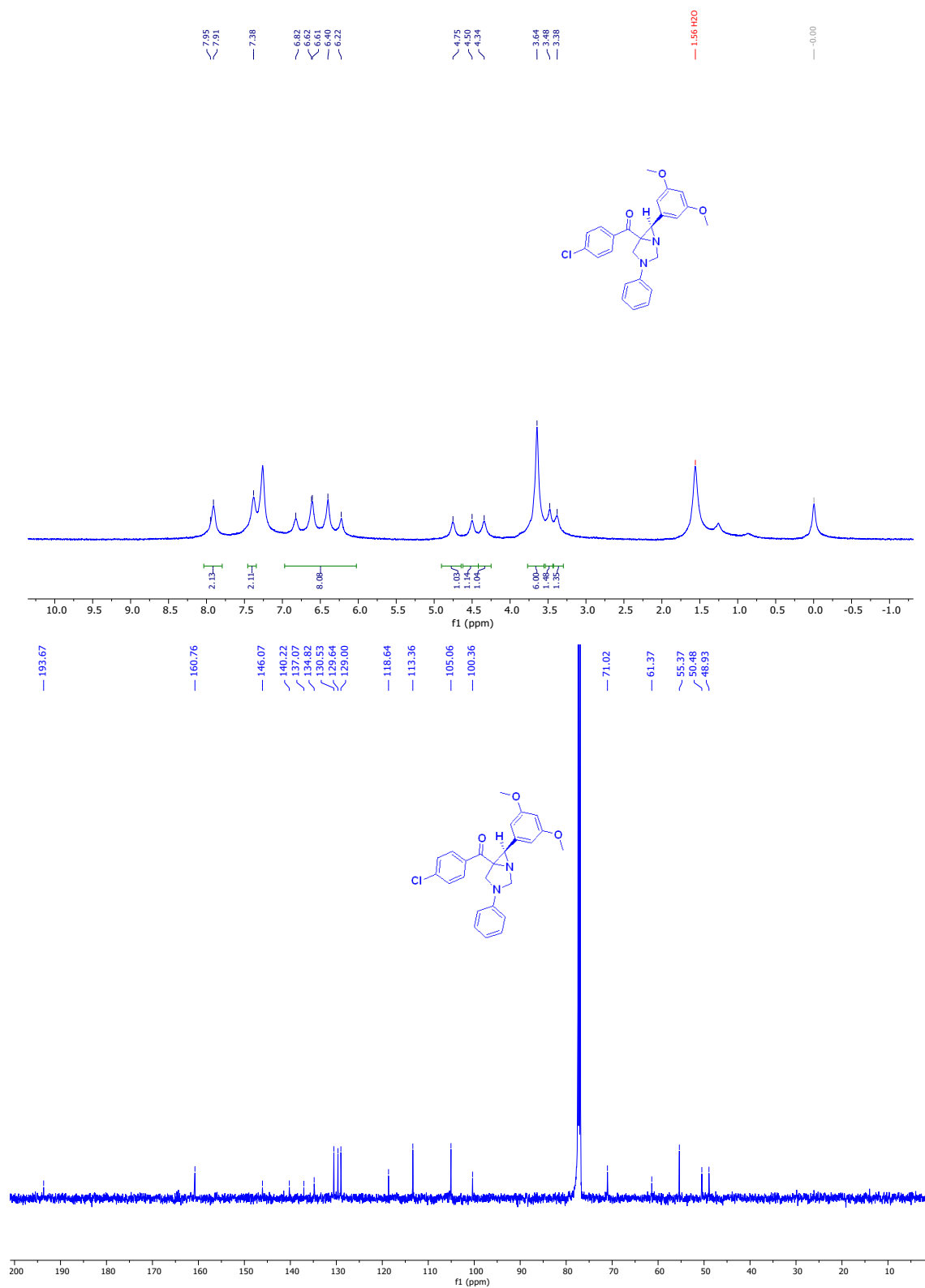
¹H NMR and ¹³C NMR Spectra of 3.6e



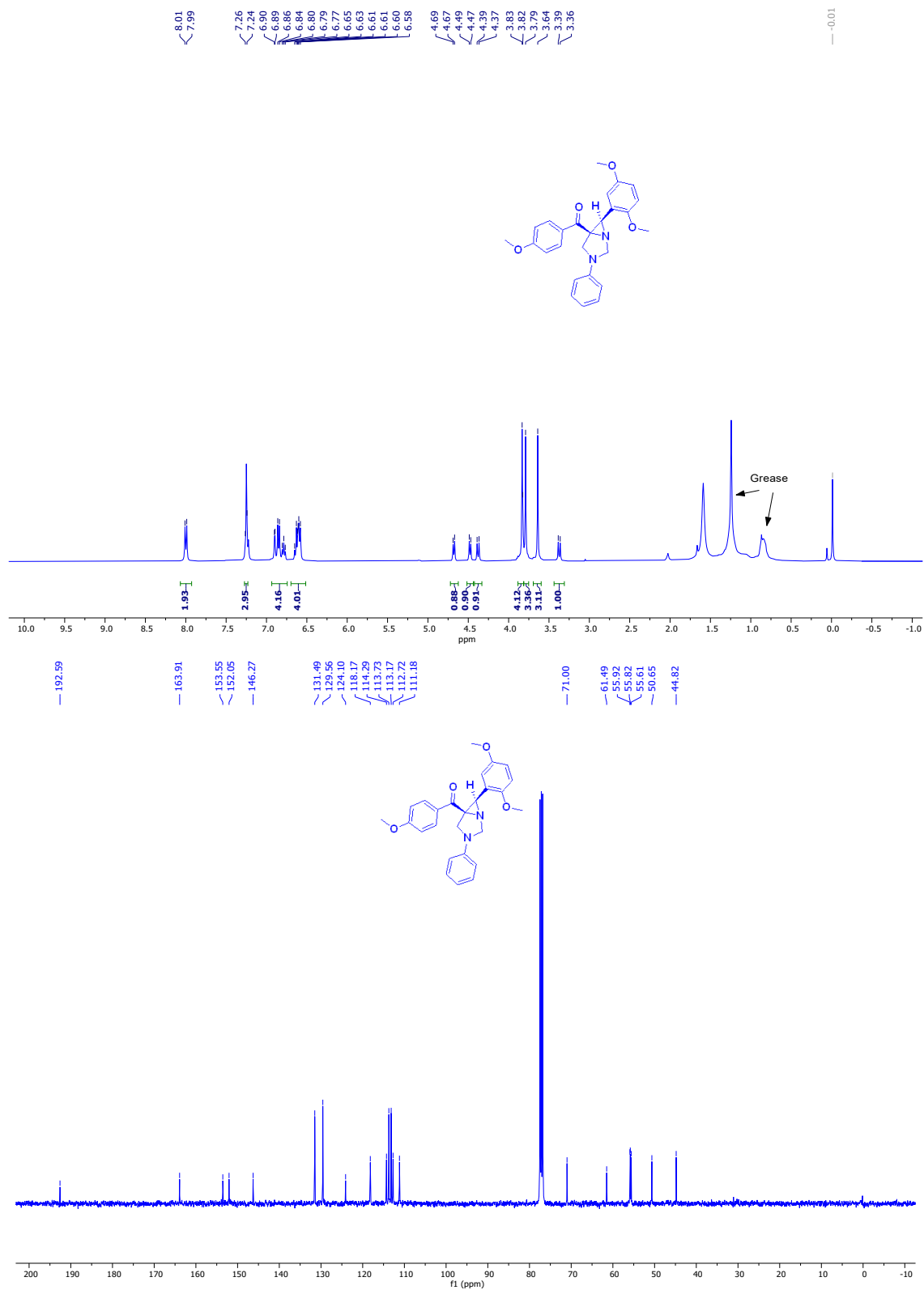
^1H NMR and ^{13}C NMR Spectra of 3.6f



¹H NMR and ¹³C NMR Spectra of 3.6g

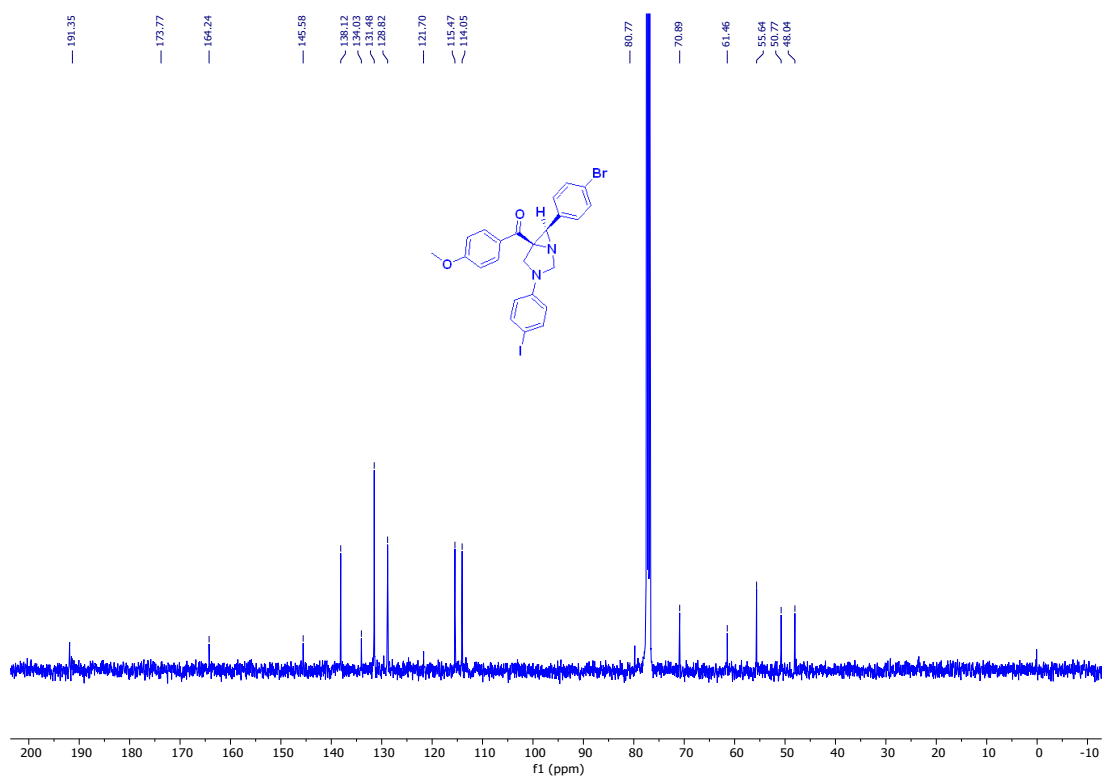
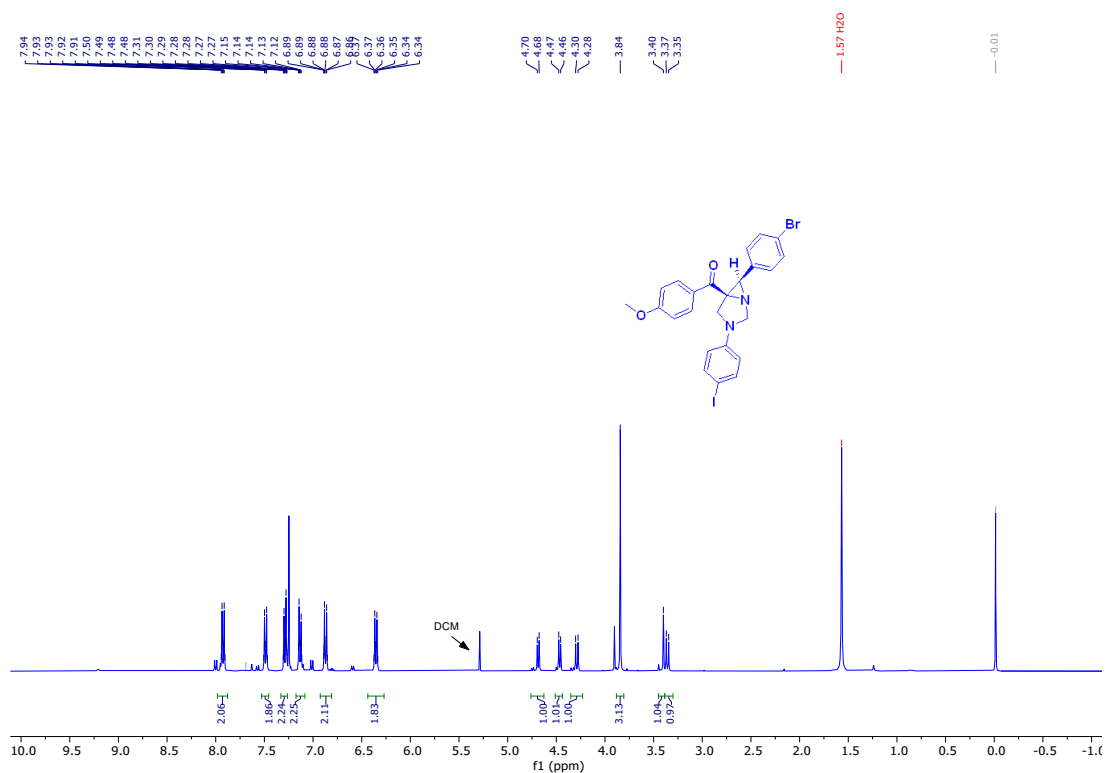


¹H NMR and ¹³C NMR Spectra of 3.6h

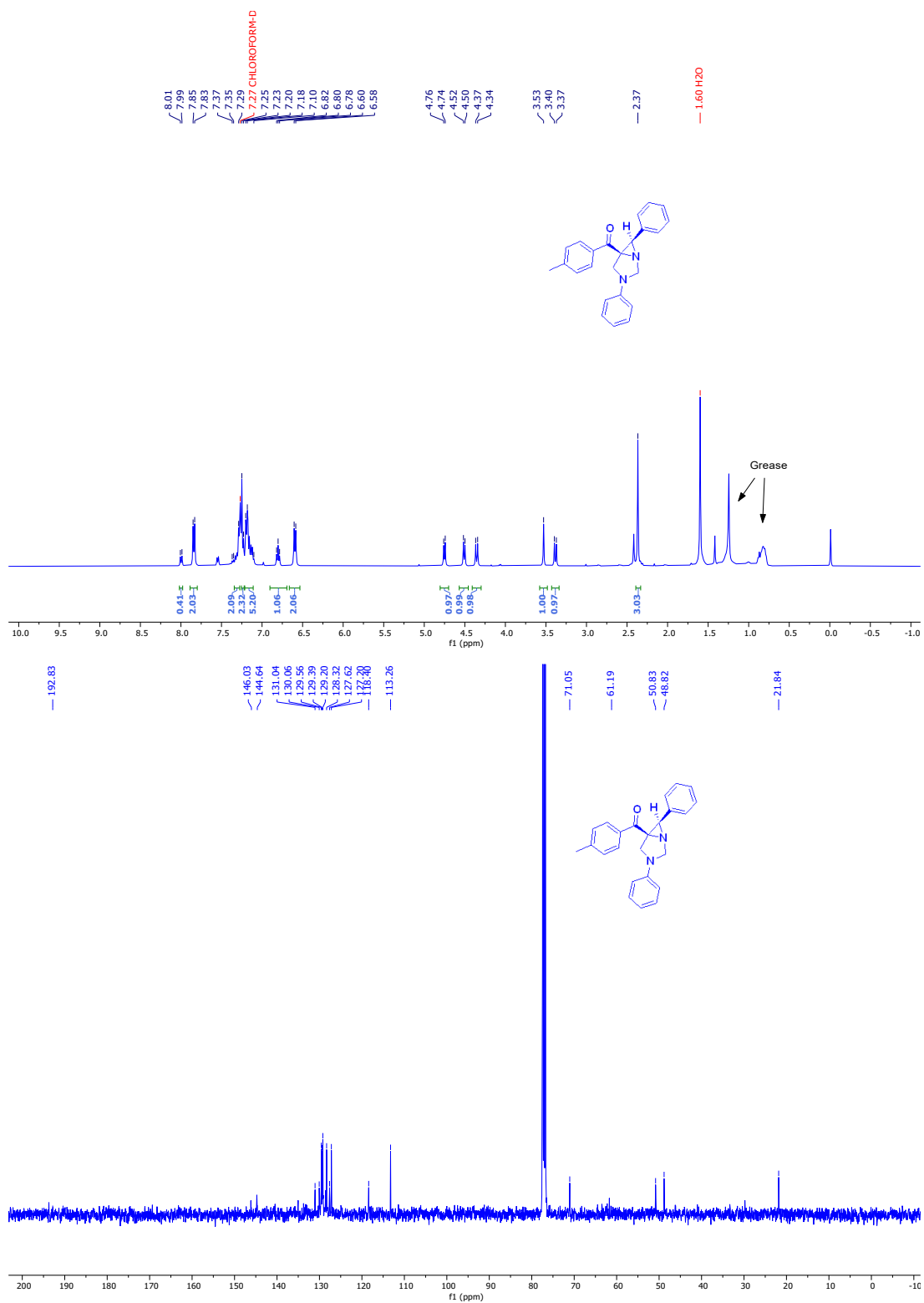


-0.01

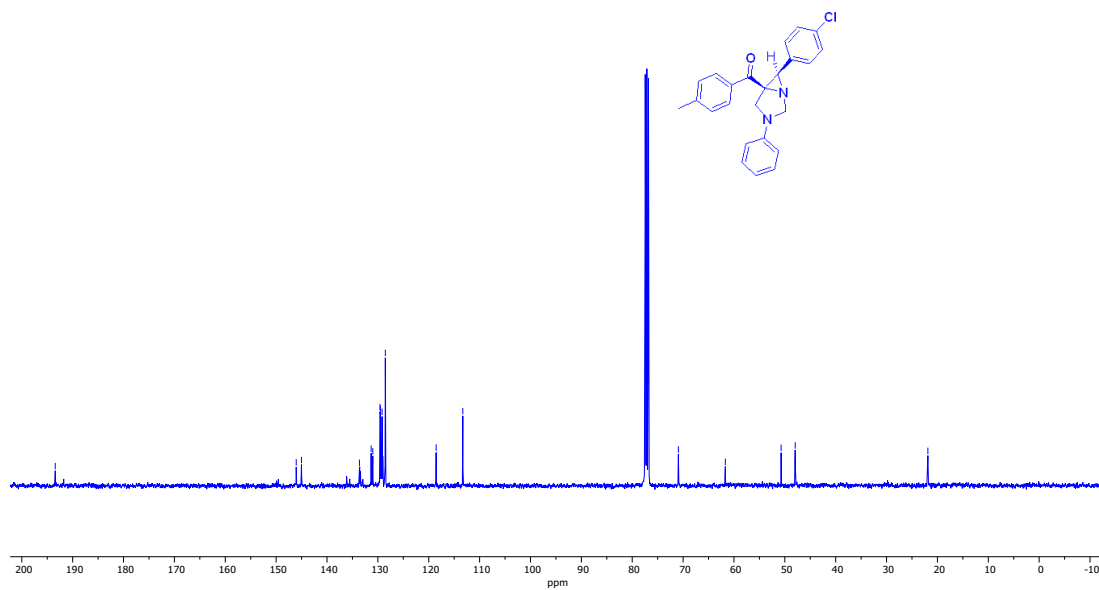
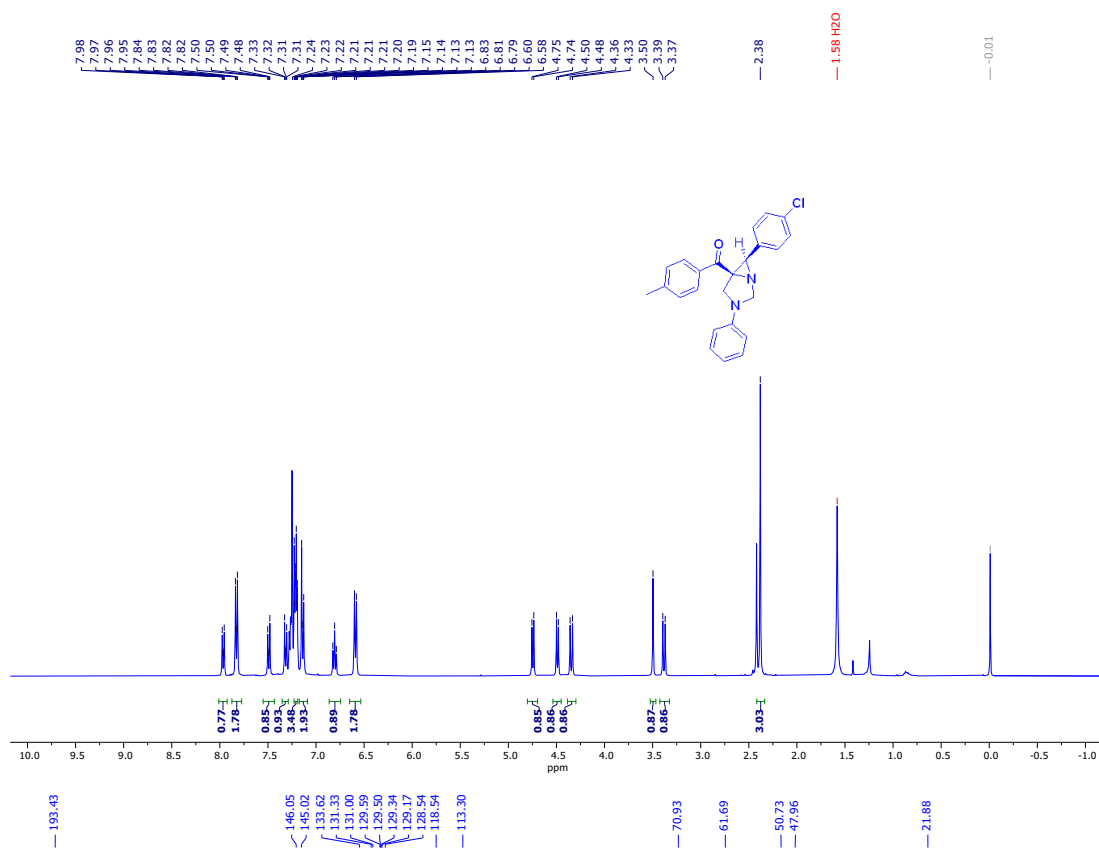
¹H NMR and ¹³C NMR Spectra of 3.6i



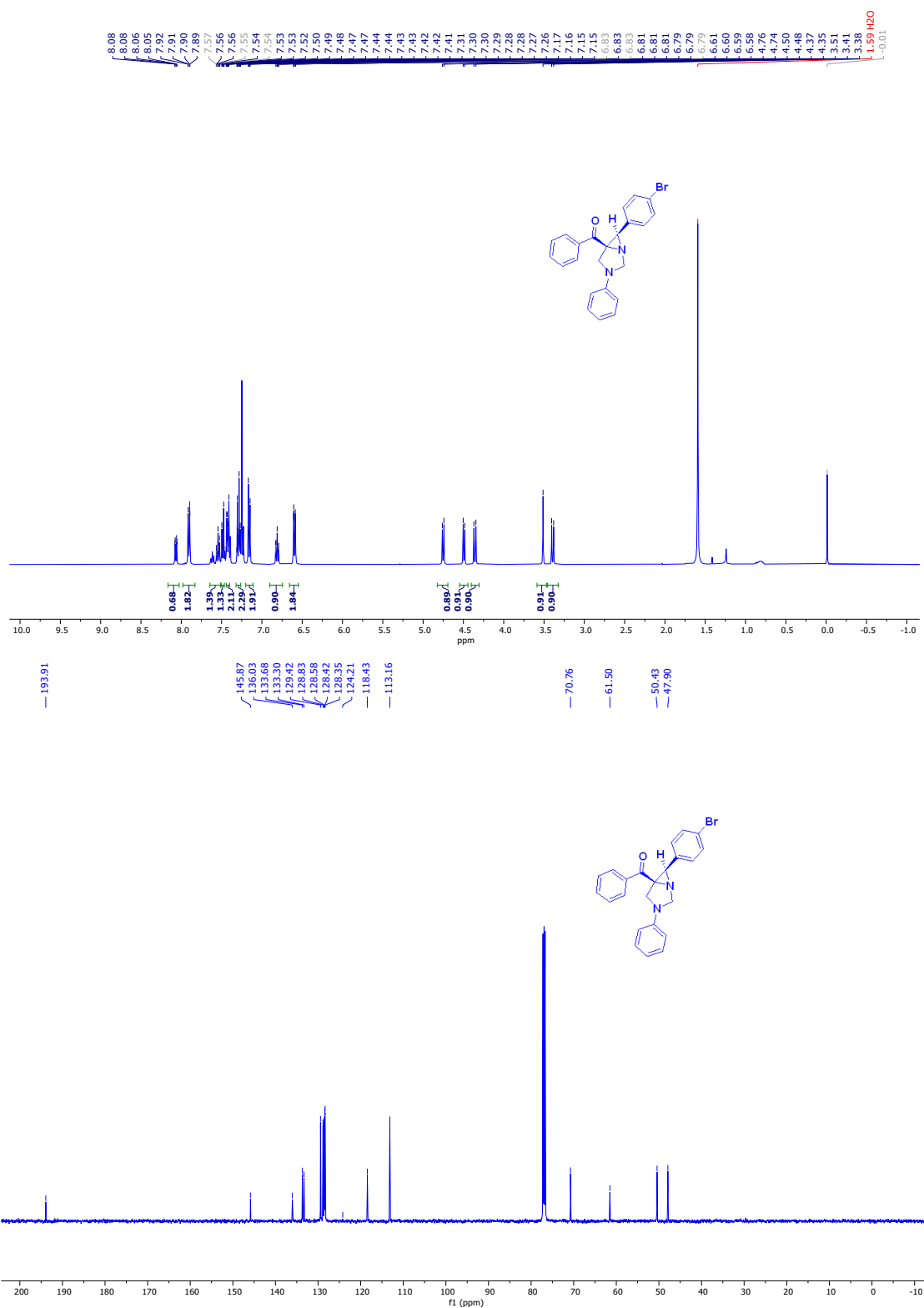
¹H NMR and ¹³C NMR Spectra of 3.6j



¹H NMR and ¹³C NMR Spectra of 3.6k



¹H NMR and ¹³C NMR Spectra of 3.61



14. Details for spectroscopic measurements and transient absorption studies

(a) Sample preparation for spectroscopic measurements

Samples were prepared by dissolving the complex in dry solvent. For steady state emission measurements, the samples were prepared using a 1 cm pathlength cuvette sealed with a rubber septum and maintained the absorbance at the excitation wavelength of 0.1 OD or below to avoid inner filter effects. The spectroscopic samples were prepared in an inert atmosphere glovebox filled with N₂. For TA measurements, the solutions were degassed with N₂ for 20 minutes before the experiments. For transient absorption measurements, the sample concentration was increased to have an OD between 0.2 and 0.3 at the excitation wavelength in a 1 mm quartz cuvette and sealed with Teflon. No photodegradation of the samples throughout the TA measurements is confirmed by the absence of any change in the absorption spectra collected before and after the experiment.

(b) Steady-state and time-resolved emission measurements

Steady state absorbance spectra are collected on a UV-Vis spectrophotometer (Cary 5000 UV-Vis NIR, Agilent Technologies). Steady state emission spectra are recorded on a steady state fluorimeter (Cary Eclipse fluorescence spectrophotometer, Agilent Technologies). Time-resolved fluorescence lifetime measurements are done using the time-correlated single photon counting (TCSPC) fluorimeter (Deltaflex, Horiba Scientific). A pulsed NanoLED centred at 401 nm, (pulse duration <1 ns; fwhm = 14 nm, 1MHz repetition rate), is used to excite the samples, and emitted photons are collected using a FluoroHub single-photon-counting detector from Horiba. The fluorescence lifetime decays are collected across the spectrum keeping the emission polarization at magic angle (54.7°) and the peak preset at 5,000 counts. The fluorescence lifetimes are obtained by fitting the lifetime decays using the commercially available using

DAS6 analysis software (Horiba Scientific) through an assessment of the goodness of its mono exponential fit by minimizing the chi-squared function (χ^2).

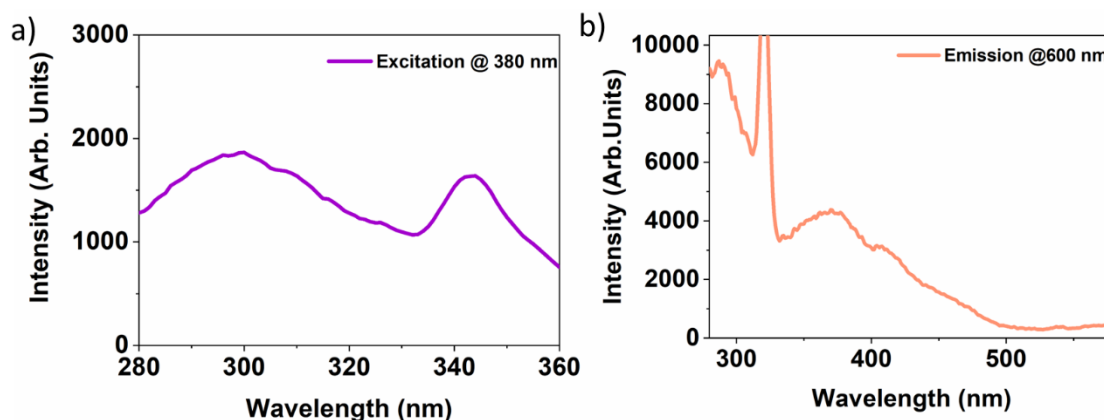


Figure 19. Steady state excitation spectrum of complex 2 in deaerated ACN at two different emission bands (a) $\lambda_{ex}= 380$ nm and (b) $\lambda_{ex}= 600$ nm.

(c) Quantum yield measurement

Steady state emission spectra were obtained on a fluorimeter. Samples were prepared with anhydrous reagent grade ACN. Emission quantum yields Φ_{em} , were measured in dilute ACN solutions at room temperature relative to $[\text{Ru}(\text{bpy})_3]\text{PF}_6$, where, $\Phi_{em}= 0.062$ in ACN⁸. The emission quantum yield was calculated using the following equation:

$$\Phi_{em} = \Phi_R \left(\frac{I}{I_R} \right) \left(\frac{A_R}{A} \right)$$

A and A_R are the absorbance of the sample at the excitation wavelengths, I and I_R are the integrated intensity of the emission band for sample and reference respectively.

(d) Stern-Volmer measurements

First, the emission spectrum of a dilute solution of complex 1 and 2 in deaerated ACN was collected. Then, appropriate amount of quencher was added to the measured solution and the emission spectrum of the sample was collected.

The dependence of the steady-state luminescence intensity on the quencher concentration [Q] in Stern-Volmer experiments is commonly described as:

$$\frac{I_0}{I_{[Q]}} = 1 + k_{SV}[Q]$$

where I_0 is the luminescence intensity in absence of any quencher, $I_{[Q]}$ the emission intensity in presence of quencher Q.

Where, τ_0 is the natural lifetime of the emissive state of the emissive species in the absence of quencher.

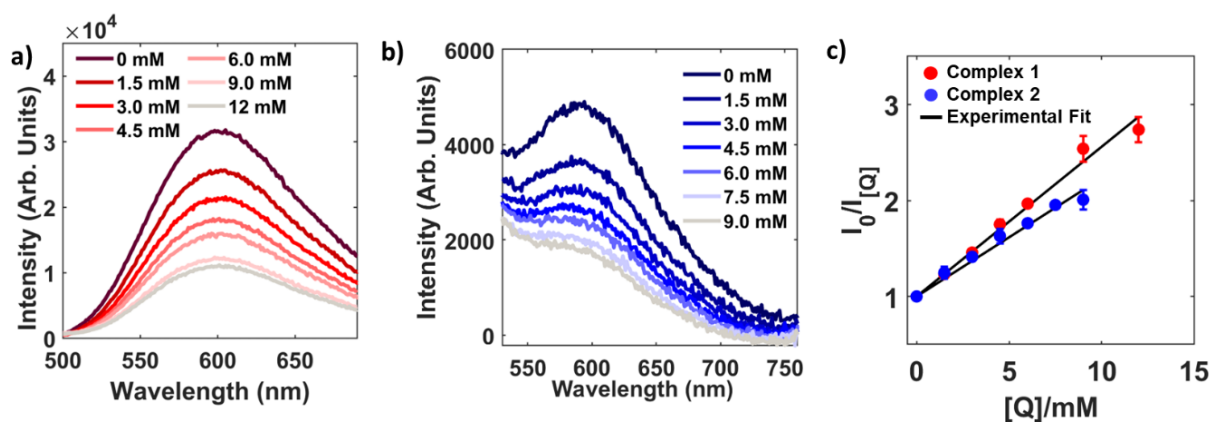


Figure 20. Steady state emission spectrum of (a) $[\text{Ir}(\text{ppy})_2(\text{bpy})]\text{PF}_6$ ($\lambda_{\text{ex}} = 355 \text{ nm}$) and (b) $[\text{Ir}(\text{ppy})_2(\text{fcbpy})]\text{PF}_6$ ($\lambda_{\text{ex}} = 400 \text{ nm}$) in deaerated ACN with increasing concentrations of N,N-dimethylaniline and (c) Comparison plot for Stern-Volmer quenching as a function of concentration of N,N-dimethylaniline, along with the experimental fit.

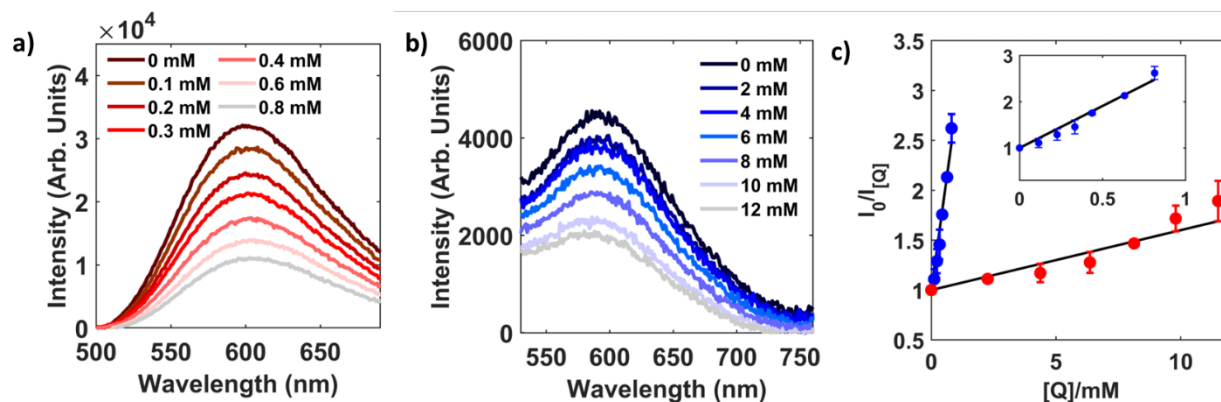
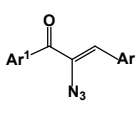
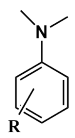


Figure 21. Steady state emission spectrum of (a) $[\text{Ir}(\text{ppy})_2(\text{bpy})]\text{PF}_6$ ($\lambda_{\text{ex}} = 355$ nm) and (b) $[\text{Ir}(\text{ppy})_2(\text{fcbpy})]\text{PF}_6$ ($\lambda_{\text{ex}} = 400$ nm) in deaerated ACN with increasing concentrations of N,N-dimethylaniline and (c) Comparison plot for Stern-Volmer quenching as a function of concentration of α -ketovinylazide along with the experimental fit.

Table S4. Time constant for Stern-Volmer and bimolecular fluorescence quenching.

S. No	Quencher	Compound	Lifetime (ns)	Stern-Volmer rate constant (k_q) M^{-1}	Bimolecular rate constant (k_{sv}) $\times 10^8 \text{ M}^{-1}\text{s}^{-1}$	R^2
1	 α -ketovinylazide	$[\text{Ir}(\text{ppy})_2(\text{bpy})]\text{PF}_6$	394	1910 ± 170	48.4	0.9664
		$[\text{Ir}(\text{ppy})_2(\text{fcbpy})]\text{PF}_6$	592	66.3 ± 1	1.11	0.9383
2	 N,N -dimethyl aniline	$[\text{Ir}(\text{ppy})_2(\text{bpy})]\text{PF}_6$	394	155.9 ± 11	3.96	0.9851
		$[\text{Ir}(\text{ppy})_2(\text{fcbpy})]\text{PF}_6$	592	123.2 ± 10	2.08	0.9724

(e) Transient absorption measurements

Femtosecond transient absorption spectroscopy was carried out on a setup that is described in detail elsewhere.⁹ In brief, Ti: Sapphire regenerative amplified femtosecond laser (Libra, Coherent) delivered fundamental ~ 55 fs pulses centred at 800 nm at 1kHz repetition rate. A portion of this fundamental output was frequency doubled by a 0.5 mm BBO crystal (type-I) to produce 400 nm excitation pump pulses. The other portion of the output was focused into a 1 mm CaF₂ crystal to obtain the continuum probe pulses. Time-resolved transient absorption difference signal (ΔA) was obtained by chopping the pump pulse with the help of a synchronized mechanical chopper at half the repetition rate of the laser. The pump was polarized at 54.7° using a half waveplate relative to the probe to minimize the influence of anisotropic dynamics on the TA measurements. A mechanical delay stage is used to control the time delay between the pump and probe pulses. The pump and probe beams were focused and crossed in a 1 mm path length sample quartz cuvette. Differential absorption spectra are collected by varying the pump-probe time delay keeping 1 sec integration time (i.e., averaging over 2000 laser shots). For transient absorption spectra, the optically induced change in the sample was described as the pump-induced absorption changes of the probe beam, where $\Delta A < 0$ represents ground state bleaching (GSB)/stimulated emission (SE) and $\Delta A > 0$ represents excited state absorption (ESA). The data are collected in four different segments at different step sizes (-1 ps to +1 ps at 0.01 ps step-size, 1.1 ps to 10 ps at 0.1 ps step-size, 11 ps to 100 ps at 1 ps step-size, 101 ps to 3000 ps at 10 ps step-size). All the measurements are carried out at room temperature, and no photodegradation of the samples is noticed after the pump-probe measurements.

(f) TA data analysis

The TA data is analyzed globally to deduce the relaxation dynamics using a free R-package TIMP software with the graphical interface program Glotaran (version 1.5.1) software.¹⁰ Note that, to account for the group velocity dispersion of the probe beam, a wavelength-dependent time-zero correction is also performed before global fitting using a free fitting software (Surface Explorer, 4.1.0 software (Ultrafast System)). Singular value decomposition (SVD) was performed on TA data set matrix $\Delta A(t, \lambda)$ to determine the number of major components that should be fitted to in the global analysis. SVD calculations showed that the data set had at least four significant components. The transient absorption spectra are globally fitted by considering a consecutive sequential relaxation model and the associated spectra are called evolution associated difference spectra (EADS) are obtained, which can be described as follows:

$$\Delta A(t, \lambda) = \sum_{i=1}^n c_i^{EADS}(t) EADS_i(\lambda)$$

where,

$$c_i^{EADS}(t) = \sum_{j=1}^i b_{ij} \exp(-k_j t) \otimes i(t)$$

$$b_{ij} = \frac{\prod_{m=1}^i k_m}{\prod_{n=1, n \neq j}^i (k_n - k_j)}$$

$i(t)$ is the instrument response function (IRF), k_j is the decay rate of component j and the amplitude b_{ji} of the exponential decay is defined for $j \leq I$ assuming $b_{11} = 1$.

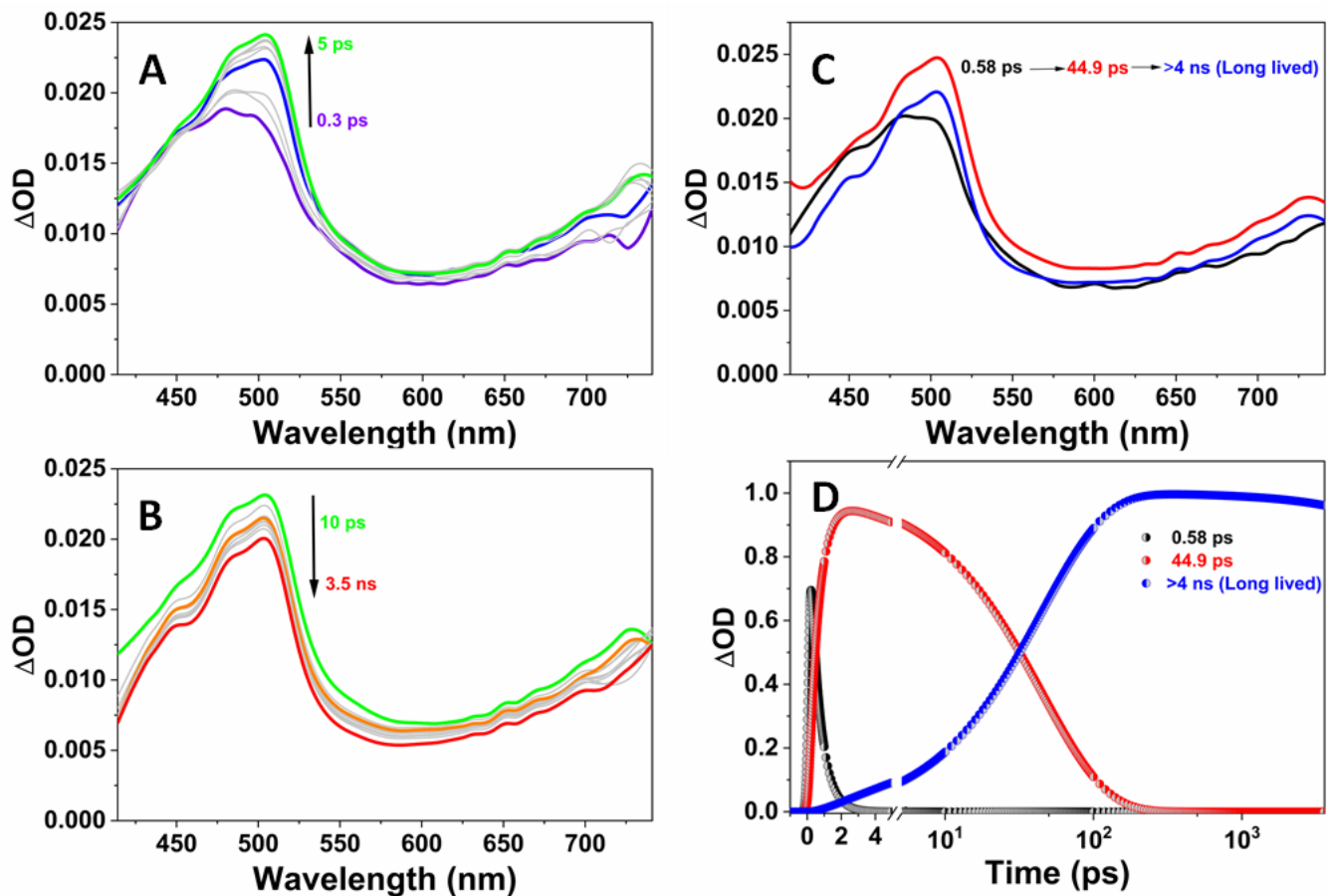


Figure S22. (a) TA spectral traces at early probe delays, (b) Spectral traces at later time delays, (c) EADS and (d) Population dynamics for complex $[\text{Ir}(\text{ppy})_2(\text{bpy})]\text{PF}_6$ in ACN following 400 nm excitation.

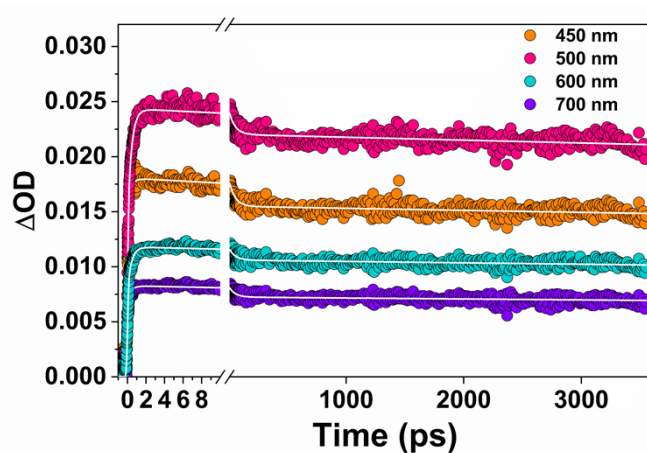


Figure S23. Kinetic traces at selected wavelengths showing the best fits for complex $[\text{Ir}(\text{ppy})_2(\text{bpy})]\text{PF}_6$ in ACN.

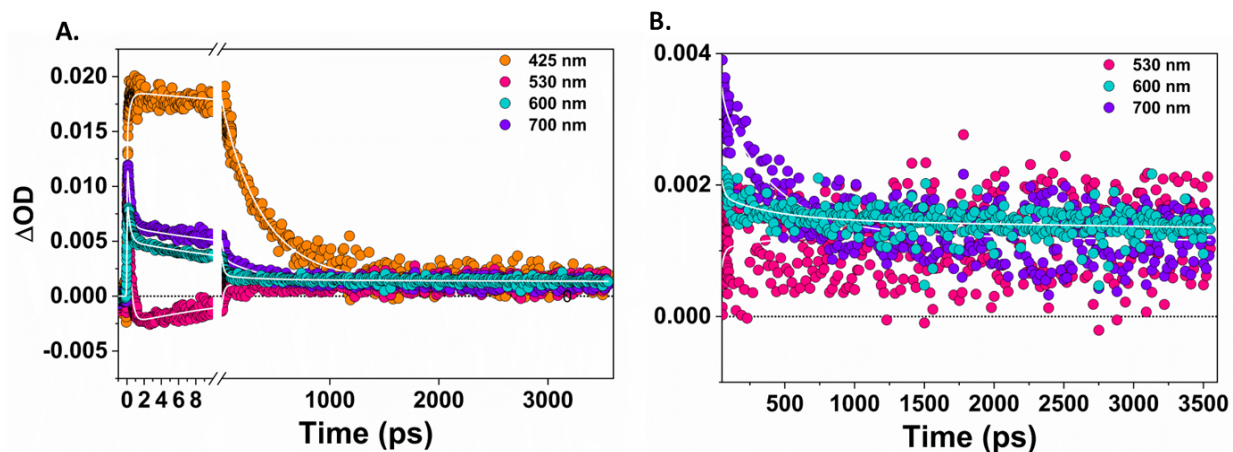


Figure S24.(a) Kinetic traces at selected wavelengths showing the best fits for complex $[\text{Ir}(\text{ppy})_2(\text{fcbpy})]\text{PF}_6$ in ACN and (b) Zoomed kinetic traces at longer time delay.

Table S5. Time constants obtained from the global analysis of the TA data.

Complex	τ_1 (ps)	τ_2 (ps)	τ_3 (ps)	τ_4^* (ns)	RMSE
$[\text{Ir}(\text{ppy})_2(\text{bpy})]\text{PF}_6$	0.58	44.9	-	394	0.0007
$[\text{Ir}(\text{ppy})_2(\text{fcbpy})]\text{PF}_6$	0.33	19.1	374.3	592	0.0006

*Time scale taken from TCSPC phosphorescence decay measurements.

PC \longrightarrow

$E_{1/2}$ of (PC ⁺ /PC) (V vs SCE)	1.06	1.25	1.21
$E_{1/2}^*$ of (PC ⁺ / [*] PC) (V vs SCE)	-1.30	-1.41	-0.96
Lifetime (ns)	592	394	557

Figure S24. The comparison of $E_{1/2}$, $E_{1/2}^*$ and lifetime of the catalysts (Ir-complexes)

15. Computational Details

All the structures are optimized using B3LYPfunctional¹¹ with Grimme's dispersion correction with Becke-Johnson Damping (D3-BJ)¹² using ORCA package.¹³The relativistic corrections are done by using Zero-Order Regular Approximation (ZORA) implemented in ORCA package.¹⁴The ZORA-Def2-TZVP basis set which uses the exponents from Def2-TZVP basis set recontracted for ZORA, is used for all the atoms except Ir for which SARC-ZORA-TZVP basis set is used.¹⁵The auxiliary basis set SARC/J is also used for Ir.¹⁶ This basis set combination referred as B1. The optimizations were carried out in an implicit solvent using CPCM solvent model,¹⁷ with parameters corresponding to acetonitrile was used to mimic the experimental condition. The natures of stationary points were characterized by frequency calculations at the same level of theory. Time-dependent density functional theory (TD-DFT) calculations were carried out at B3LYP/B1 level to calculate the absorption spectra of the complex. The lowest 100 transitions, up to 240 nm, were taken into account in the calculations of the absorption spectra.

15. References

- ¹T. B. Rauchfuss, *Inorg. Synth.*, 2010, **35**, John Wiley & Sons.
- ²SAINT+software for CCD diffractometers, Bruker AXS, Madison, WI, 2000.
- ³G. M. Sheldrick, SADABS Program for Correction of Area Detector Data, University of Göttingen, Göttingen (Germany), 1999.
- ⁴SHELXTL Package v. 6.10, Bruker AXS, Madison, WI, 2000; G. M. Sheldrick, SHELXS-86 and SHELXL-97, University of Göttingen, Göttingen (Germany), 1997.
- ⁵K. Brandenburg, Diamond, v3.1e, Crystal Impact GbR, Bonn, Germany, 2005.
- ⁶R. A. Maurya, P. R. Adiyala, D. Chandraskhar, C. N. Reddy, J. S. Kapure, A. Kamal, *ACS Comb. Sci.*, 2014, **16**, 466–477.
- ⁷(a) P. A. S. Smith, *Open-Chain Nitrogen Compounds*, Benjamin, New York, 1966, **2**, 211; (b) J. H. R. Boyer, B. Moriarty, D. Darwent, P. A. S. Smith, *Chem. Eng. News*, 1964, **42**, 6.
- ⁸J. M. Calvert, J. V. Caspar, R. A. Binstead, T. D. Westmoreland, T. J. Meyer *J. Am. Chem. Soc.* 1982, **104**, 24, 6620–6627.
- ⁹(a) S. Dhamija, B. Thakur, P. Guptasarma, A. K. De, *Faraday Discuss.* 2018, **207**, 39-54; (b) Y. Silori, S. Chawla, A. K. De, *Chem. Phys. Chem.* 2020, **21**, 1908-1917.
- ¹⁰(a) H. M. van Stokkum, D. S. Larsen, R. van Grondelle, *Biochim. Biophys. Acta*, 2004, **1657**, 82-104. (b) J. J. Snellenburg, S. P. Liptonok, R. Seger, K. M. Mullen, I. H. M. van Stokkum, *J. Stat. Software*, 2012, **49**, 1-22.
- ¹¹A. D. Becke, *Phys. Rev. A: At., Mol., Opt. Phys.*, 1988, **38**, 3098. (b) A. D. Becke, *J. Chem. Phys.* 1992, **96**, 2155. (c) A. D. Becke, *J. Chem. Phys.*, 1993, **98**, 5648.
- ¹²S. Grimme, S. L. Ehrlich, L. Goerigk, *J. Comput. Chem.*, 2011, **32**, 1456.
- ¹³(a) F. Neese, *Wiley Interdiscip. Rev.: Comput. Mol. Sci.*, 2012, **2**, 73. (b) F. Neese, *Wiley Interdiscip. Rev.: Comput. Mol. Sci.*, 2018, **8**, e1327.
- ¹⁴(a) E. van Lenthe, J. G. Snijders, E. J. Baerends, *J. Chem. Phys.*, 1996, **105**, 6505. (b) C. van Wuellen, *J. Chem. Phys.*, 1998, **32**, 392.

¹⁵(a) F. Weigend, R. Ahlrichs, *Phys. Chem. Chem. Phys.*, 2005, **7**, 3297. (b) F. Weigend, M. Haser, H. Patzelt, R. Ahlrichs, *Chem. Phys. Lett.*, 1998, **294**, 143. (c) D. A. Pantazis, X. Y. Chen, C. R. Landis, F. Neese, *J. Chem. Theory Comput.*, 2008, **4**, 908.

¹⁶(a) D. A. Pantazis, F. Neese, *J. Chem. Theory Comput.*, 2009, **5**, 2229. (b) D. A. Pantazis, F. Neese, *Theor. Chem. Acc.*, 2012, **131**, 1292. (c) D. A. Pantazis, F. Neese, *J. Chem. Theory Comput.*, 2011, **7**, 677.

¹⁷V. Barone, M. Cossi, *J. Phys. Chem. A*, 1998, **102**, 1995.